2016

Shortened Poly-N-Acetyl Glucosamine (sNAG) Nanofibers Induce Rapid Vascular Assembly in 3-Dimensional Microtissue Spheroids

Michael G. Sarson
Medical University of South Carolina

Shortened Poly-N-Acetyl Glucosamine (sNAG) Nanofibers Induce Rapid Vascular Assembly in 3-Dimensional Microtissue Spheroids

BY

Michael G. Sarson

A thesis submitted to the faculty of the Medical University of South Carolina in partial fulfillment of the requirements for the degree of Master of Biomedical Science in the College of Graduate Studies

Department of Regenerative Medicine and Cell Biology

2016

Approved by:

Chairman, Advisory Committee _____

_____

_____

_____

_____

Table of Contents

List of Figures

List of Abbreviations

3D – three-dimensional

AoAF – aortic adventitial fibroblast

ADSC – adipose-derived stem cell

a-SMA – alpha smooth muscle actin

CVD – cardiovascular disease

ESC – embryonic Stem Cell

ECM – extracellular matrix

EC – endothelial cell

HF – heart failure

HSP – heat shock protein

iPSC – induced pluripotent stem cell

LVAD – left ventricular assist device

MI – myocardial infarction

MMP – matrix metalloproteinase

MPCs – myocardial progenitor cell

MSC – mesenchymal stem cell

PECAM – platelet endothelial cell adhesion molecule

pGlcNAc – poly-N-acetyl glucosamine

sNAG – shortened poly-N-acetyl glucosamine

TGF-b – transforming growth factor

UCB-EPC – umbilical cord blood-endothelial progenitor cell

VEGF – vascular endothelial growth factor

VSMC – vascular smooth muscle cell

Abstract

Tissue vascularization and integration with host circulation remains a key barrier to the successful translation of engineered tissues into clinically relevant therapies. Current efforts to implant large engineered structures are limited by insufficient delivery of oxygen and nutrients, and waste removal. Work presented in this thesis focus on the use of a naturally derived nanofiber for improving molecular interactions between vascular endothelial cells and smooth muscle cells for application to vascular bioengineering. We hypothesize optimization of instructive interactions between vascular cell types can improve formation of microtissue spheroids for application to vascular bioengineering. Toward this goal, I use shortened poly-N-acetyl glucosamine (sNAG) nanofibers to facilitate co-assembly of pre-vascularized network formation within microtissue spheroids. To gain initial insights into the potential use of sNAG as an instructive biomaterial for vascular tissue regeneration applications, UCB-EPCs, ADSC-VSMCs, and AoAFs were co-cultured in cell-aggregates in the presence of sNAG or other known effectors of vascular assembly. Immunofluorescence analysis by confocal microscopy revealed a strong angiogenic effect on EC-only monocultures, which resulted in EC sprout formation, and remodeling in 2D Matrigel assays. When grown in 3D, sNAG nanofibers induced UCB-EPCs migration and increased levels of hPECAM-1 expression, indicative of a fully differentiated EC phenotype. Heterotypic cell cultures show that sNAG nanofibers elicit synthesis of proteins associated with vascular wall assembly and stabilization. An interesting finding of these analyses was that expression of collagen type-4 was significantly increased in our sNAG treated microtissue spheroids.

This increase was greatest in areas of heterotypic cell association, highlighting the importance of cross talk between EPC-ECs and ADSC-VSMCs in stimulating synthesis of vascular wall components. Collectively, our preliminary studies suggest that sNAG nanofibers may provide an instructive, biocompatible matrix for assembly of prevascularized microtissue spheroids.

BACKGROUND

Cardiovascular disease (CVD) is the leading cause of morbidity and mortality worldwide. [1, 2] In the United States, cardiovascular diseases account for approximately 30% of all deaths, with CVD population constantly increasing. In 2008 alone, 86.2 million Americans were living with some form of CVD, and this number is projected to grow to 40.5% of the American population by the year 2030. Concomitantly, the financial burden of disease is also projected to rise, from present estimates of $300 billion to $800 billion. [3] On a global scale, CVD is responsible for 60% of deaths, and will become increasingly important as global obesity and malnutrition continue to rise. Importantly, CVD is responsible for 80% of non-communicable disease in low and middle-income countries, with grave social and economic consequences.

Unfortunately, despite this epidemic of increasing amounts of CVD, the myocardium has very limited capacity to repair itself following injury compared to other tissues. Two distinct cardiac pathologies that lead to coronary heart disease are myocardial infarction (MI) and diabetic cardiomyopathy (DCM). In both cases, injury occurs when a coronary artery becomes obstructed and tissue downstream of the occlusion begins to die due to lack of oxygen. As a result, cardiac injury triggers a pathologic adaptive cascade that occurs in three phases. The first is the inflammatory phase, occurring hours to days after injury, in which cardiomyocyte death leads to the release of chemokines and cytokines that recruit inflammatory cells to the site of injury. This is followed by the proliferative phase (days to weeks), which is characterized by a

high degree of angiogenesis and mesenchymal cell recruitment to the site of injury. The third and final phase is maturation of the scar tissue as the newly deposited ECM is cross-linked and the majority of fibroblasts and endothelial cells present in the previous phases undergo apoptosis. Subsequent formation of scar tissue during the final stage of the healing process results in maladaptive stiffening of the ventricular wall, which lacks the contractile, mechanical, and electrical properties of the healthy myocardium. This loss of function leads to further injury and subsequent progression into heart failure (HF).

HF is a clinical syndrome characterized by systemic perfusion inadequate to meet the body's metabolic demands as a result of impaired cardiac pump function. Contemporary treatments such as surgical, endovascular, and pharmacological interventions are merely palliative in nature and do not adequately address the true cause of heart failure – the loss of functional myocytes and supporting cardiac tissue. At present, the only available treatment option for end-stage HF is the Left Ventricular Assist Device (LVAD); however, this device is generally intended for temporary use until the patient can receive a full heart transplantation. As such, heart transplantation remains the gold standard of care and the only curative therapy for replacing damaged or diseased myocardium as a result of vascular insufficiency. Unfortunately, the current availability of replacement hearts has become exceedingly limited due to a consistent and growing gap between the number of patients waiting for organs and those available. In 1991, 68% of patients on the waiting list received replacement hearts.[4] As of 2013, this number dropped to 24% of patients on the waiting list [4], highlighting the

critical clinical need for innovative therapies that address the progression of pathological remodeling and cell death, as well as to repair/regenerate the affected areas.

Cell-Based Therapies for MI

The emerging of cardiovascular regenerative medicine may provide an encouraging direction for future therapeutics, which focuses on replacing or regenerating damaged myocardium, blood vessels, and microvasculature to restore or establish normal cardiac function.[5, 6] Besides cardiomyogenesis, cardioprotective mechanisms, including anti-fibrosis, anti-inflammation, and neovascularization, have been shown to play critical roles in cardiac repair following an ischemic event. [7] These mechanisms represent promising therapeutic targets and can be exploited for regenerative potential. This theory is supported by recent evidence that suggests myocardial progenitor cells (MPCs) do not result in the formation of functional syncytia and that their effects in post-MI scarring might be mediated more by local paracrine angiogenesis than by cardiomyocyte differentiation. [8, 9] Hence, angiogenesis might constitute an important mechanism of functional improvement not only among modalities that specifically aim at angiogenesis (ie. for the treatment of myocardial ischemia in the presence of viable heart muscle), but also among modalities aiming at myogenesis to improve cardiac function after an MI (i.e. for the treatment of heart failure in the presence of nonviable myocardium). [10-12] Therefore, the ability to

induce angiogenesis or vasculogenesis via supplementation of vascular cell types could provide an effective strategy for achieving post-MI recovery.

Adult stem cells hold great potential to repair damaged heart tissue and can be utilized as treatment to accelerate healing through potent paracrine signaling, with a production of a multitude of proangiogenic factors, or by restoring tissue function by direct contribution to neovascularization. Many clinicians prefer to utilize autologous adult stem cells due to the relative low cost and safety as compared to embryonic stem cell (ESC) or induced pluripotent stem cell (iPSC) use. Adult stem cells, unlike embryonic stem cells, are not derived by sacrificing an embryo, thus avoiding many of the ethical controversies involved in embryonic stem cell research. In fact, the therapeutic application of adult stem cells is further along in clinical development than any other stem cell approaches. [13] By contrast to ESCs or iPSCs, adult stem cells are partially lineage-committed and therefore have the capacity to give rise only to cells of a given germ layer. In other words, they are multipotent, rather than pluripotent, which reduces the likelihood of teratoma formation in vivo. [14] Although adult stem cells have a lower renewal capability than ESCs and iPSCs, they have a greater proliferation rate than terminally differentiated somatic cells, thus still benefiting regenerative medicine approaches.

Several groups have demonstrated that adult stem cells are capable of differentiating into a variety of essential vascular cell types, including endothelial cells, as well as surrounding mural support cells required for vascular stability. Mural cells, commonly referred to as vascular smooth muscle cells (SMCs) in larger vessels and

pericytes, in capillary beds are indispensable for the development of a mature and durable vasculature. The importance of these cells is underscored by gene mutation studies of mouse models where the absence of mural cells resulted in severe vascular defects. [15-17] Other in-vivo studies have focused on the transplantation of harvested progenitor cells, namely EPCs, into animal models of myocardial infarction or hindlimb ischemia. In this context, hybrid cellular approaches have demonstrated greater success than using single cell types. Co-implantation of mouse mesenchymal precursor cells and human EPCs sustained long term durability of engineered vascular networks while implantation of ECs alone led to vessel regression within a week. Inclusion of mouse embryonic fibroblasts in addition to human EPCs and mesenchymal cells enhanced the viability of vascularized cardiac muscle patches, which integrated stably onto murine myocardia. Thus, ECs and mural cells are both unequivocally necessary for the formation of a functional vasculature.

Despite the impressive in vivo potential of adult stem cell-based therapy, several obstacles (e.g., the difficulty of maintaining self-renewal and poor survival due to apoptosis and/or necrosis at the administration site) have been encountered. [18] The primary limitation is the poor viability (low survival rates) of the transplanted adult stem cells by anoikis in injured tissues. Anoikis is a form of programmed cell death that occurs due to the loss of anchorage-dependent attachment to the extracellular matrix (ECM). [19, 20] Because cell-cell adhesion through the ECM plays an important role in cell activities, proliferation, and survival, [21] a low propensity to adhere to the host cells due to a loss of matrix anchorage may induce the death of the transplanted adult stem

cells. Although several ongoing studies are focused on improving adult stem cell survival, no potential solutions have been suggested to solve the underlying problem of weak adhesion. Therefore, enhancing the adhesion of the transplanted adult stem cells through the inhibition of anoikis should improve the success of adult stem cell-based applications. [21]

Biomaterials for Enhancing Stem Cell-based Transplantation

Biomaterials made of both synthetic and natural polymers have gained much attention in recent years due to their ability to modulate cell behavior. These materials can be designed to create a well-defined microenvironment in the tissue that can specifically direct cell attachment and regenerative potential, and may be useful for improving outcomes of stem cell-based therapies. In particular, biomaterials can control the release of growth factors and cytokines in a spatiotemporally regulated manner to mimic endogenous signals that cells use for specific processes, and the concentration can be tuned to levels effective for promoting the desired behavior. (MMP Sensitive) The advantage of using biomaterials for stem-cell delivery is that they provide initial encapsulation of the donor cells and gradually precondition the cells to the local biological environment for which they will be implanted. Furthermore, biomaterials such as alginate-based microcapsules can play an immunoprotective role by isolating the donor cells from the host immune system and thus increase allogeneic cell transplantation tolerance. [17, 22]

Vascular progenitor cells can also be used to vascularize tissue patches or construct vascular grafts. The ideal scaffolds for engineered tissue patches and vascular grafts are usually composed of biomimetic ECM components. The presence of ECM can encourage the maturation of newly formed blood vessels. The spatial complexity of ECM creates defined topological cues that can regulate vascular specification and organize vascular cells into tube-like structures.[23] Physical contacts with the ECM also modulate biophysical signals between the dynamic biological environment and the donor cells, leading to better viability, engraftment and patency of vascularized tissue patches or vascular grafts after implantation. A recent study by Xiong et al. reported that the use of a porous fibrin biomatrix promoted significant engraftment of vascular progenitor cells in a swine model of myocardial infraction. [24] Nevertheless, there are only a few studies on biomaterial-assisted generation and transplantation of vascularized tissue patches or vascular grafts using progenitor cells. [17] The vascularization process is typically too slow to maintain the viability of the therapeutic cells of interest, and only tissues with low vascularization requirements, such as thin skin tissue or cartilage, are currently available clinically.

Most of the current vascularization approaches have proven successful in inducing blood vessel formation in vivo, but many of these blood vessels are not fully functional (leaky or not connected to the host vasculature), and many regress over time. Where some of these approaches have resulted in a functional, persistent blood vessel network, the time required to achieve such functional vascularization is still too long to be clinically relevant (several weeks for a millimeter sized implant). [25] Without an

immediate vascular supply, the majority of the therapeutic cells within the construct will not survive. Going forward, much effort will need to be directed towards accelerating the formation of a perfused (i.e. anastomosed) vascular network within the construct and ensuring the new vasculature matures and persists.

Modular Tissue Engineering

In order to enhance the function of bioengineered tissues, there is a need to generate more complex structures with features such as developed and functional microvasculature and tissue specific morphology. The emerging field known as modular tissue engineering aims to accomplish these goals by fabricating microtissue building blocks with intricate architectural features and using these modular units to engineer biological tissues from the bottom up. These modules can be created in a number of ways, such as through self-assembled aggregation, [26] microfabrication of cell-laden hydrogels, [27] creation of cell sheets, [28] or direct printing of tissues. [29] Once created, these modules can be assembled into larger tissues through a number of methods such as random packing, [30] stacking of layers, [28, 31] or directed assembly. [32] By mimicking native microstructural functional units, bottom-up approaches have the ability to create more viable engineered tissues.[33, 34]

The historical roots of the modular approach trace back to microencapsulation techniques, such as encapsulating pancreatic islet cells in alginate gels for transplantation in diabetic rats.[33] More recent studies focus on exploiting the intrinsic vascularized nature of the modular approach by incorporating vascular supporting cells

(such as smooth muscle cells, (SMC), or mesenchymal stromal cells, (MSC)) or therapeutic cells of interest (cardiomyocytes, islets, or others), to be embedded inside the modules. A significant advantage of this approach is that modules containing different supporting or therapeutic cells can also be mixed together in a desirable ratio to build more complex functional tissue structures. Another advantage of this approach is that the modular design allows for uniform cell seeding (by controlling the cell density within each of the individual modular building blocks), as well as controlled mixing of different cell populations (by mixing together modules encapsulating different functional cells, in different ratios), and is scalable (increasingly larger tissue constructs can be made by assembling increasing numbers of modular building blocks.) The three-dimensional tissues assembled using this method have an intrinsic vasculature, are scalable, have uniform cell density throughout the construct, and allow for the mixing of different cell types within the modules or by using modules with different types of embedded cells, thus avoiding common limitations of conventional scaffolds and fabrication techniques.

The major challenge to advance this modular approach has been to improve or develop new methods for assembling modules in a more precise and controlled manner. The other challenge has been to improve the resolution of the assembled 3D constructs by making better reproducible modules of even smaller dimensions. The mechanical properties of the modular scaffolds can be improved by more conventional methods like introducing fibers or membranes to support the modular constructs.

Nanofibers for Modular Tissue Engineering

Recent advances in nanotechnology and material science have made nanofiber polymers an attractive choice among biomaterials for enhancing biological and mechanical properties of modular tissue engineering strategies. Polymeric nanofibers have proven to be excellent substrates for cell attachment and growth, and the microstructure of polymeric nanofiber grafts can predictably modulate cell behaviors such as morphology, differentiation, ECM deposition, and migration. This nanofibrous ECM provides mechanical strength, storage locations for biomolecules, and also provides a template for tissue formation in development, regeneration, and remodeling. Other properties of nanofiber polymers make them well suited for more specific applications; for example, nanofibers may offer more physiologic mechanical properties for load bearing tissues, directional alignment to structures with aligned morphologies, and nanofiber meshes with fine pores act as membranes that allow transport of nutrients and waste. Despite the advantages, key scientific issues, such as the effects of ECM composition and temporal-spatial effects of ECM materials on stem cell differentiation, still need further investigation.

Challenges in translating these technologies to the clinical arena include optimizing substrate topographical cues to promote desired cell responses and the ability to design scaffolds with architecture conducive to the formation of tissue-like structures in vitro and in vivo. Although nanotopography can affect cellular behavior through known mechanisms such as regulation of cell shape and surface protein absorption properties, it is also possible that there are unknown effects associated with

nanotopographys as well. Cells can react to objects as small as 5nm and it is possible that nanostructures, especially those with similar dimensions to natural ECM, can negatively influence cell behavior resulting in undesired clinical outcomes. It has been shown that cell behavior can be highly dependent on the substrate that they are cultured on, and the understanding of cell-substrate interactions with nanostructures could provide valuable information that would allow for the design of more effective scaffolds.

sNAG as a novel nanofiber substrate for Vascular Engineering

The design and selection of a biomaterial is a critical step in the development of scaffolds for tissue engineering. [35] Studies have shown that nanofiber polymers of natural origin are among the most attractive options, mainly due to their similarities with the ECM, chemical versatility as well as typically good biological performance. [35] A recent development in the design of naturally derived polymers is the large-scale isolation and purification of poly-N-acetyl glucosamine or pGlcNAc from a marine microalga by Vournakis et al. [36] These pure nanofiber preparations have been tested for their biocompatibility and show no toxic, allergic or deleterious effects and are therefore considered completely biocompatible. These features make them an ideal candidate for enhancing modular tissue engineering approaches.

Previous studies have shown that pGlcNAc nanofiber-derived membranes promote accelerated wound healing in both wild type animals and in those with delayed wound healing phenotypes. Increased wound repair mediated by nanofiber treatment is

characterized by increased hemostasis [37, 38] , re-epithelialization, granulation tissue formation and angiogenesis [39]. Expression of markers of angiogenesis [40, 41] (VEGF), cell migration (uPAR) and ECM remodeling (MMP3, MMP9) were also up-regulated in sNAG treated wounds compared with controls. Mechanistic studies by our laboratory using these nanofibers in vitro and in vivo, have shown that due to their unique three-dimensional structure, these fibers directly bind to and stimulate integrin mediated outside-in signal transduction that is, at least in part, dependent on Akt1 activation in EC and in fibroblasts. In EC, we have shown that nanofiber stimulation results in increased metabolism [42] enhanced innate immune responses leading to antibacterial activity, and to increased endothelial cell motility and angiogenesis [43]. In addition to changes in activation of transcription factors such as Ets1 and PGC1a, nanofiber stimulation results in marked increases in VEGF expression and interleukins such as IL-1 [40].

pGlcNAc nanofiber-treated wounds were also shown to exhibit reduced scarring, increased tensile strength and elastic modulus compared to untreated wounded skin and this corresponds with higher collagen and elastin content as determined by hydroxyproline analyses and immunohistological examination. We also observed increased tropoelastin staining in sNAG treated cells. These findings suggest that sNAG treatment results in increased tensile strength as well as increased elasticity and supports the theory that nanofiber treatment decreases scarring while concurrently increasing the mechanical properties of healing tissue. Importantly, these effects are correlated with increased angiogenesis and vascular cell signaling. In control experiments, compounds containing similar repetitive sugar moieties lacking sNAG

specific nanofiber structure (e.g. chitin/chitosan which have a B-sheet-type structure) do not possess this biological activity [44, 45]. These findings suggest that pGlcNAc nanofibers can be used to not only provide an optimal substrate for cell attachment and growth, but also improve the mechanical integrity of modular tissue-engineering strategies; thus providing combinatorial advantages using a single biomaterial.

CHAPTER 2: THESIS OVERVIEW

Goal: Augment tissue regeneration by rapid anastomosis of engineered autologous microtissues with host vasculature.

Objective: Develop biomaterial-based strategies to build vascularized modular tissue engineered constructs.

Approach: Our approach involves the combination of adult stem cells (i.e. UCB-EPCs, ADSC-VSMCs) with AoAFs, to be used for generation of pre-vascularized microtissue aggregates. Preliminary results show that this type of spheroid-based approach elicits increased synthesis and secretion of vascular ECM, including elastin, which is not typically expressed in post-natal VSMCs, thus highlighting the importance of heterotypic interactions between ECs and VSMCs for increased mechanical strength and stiffness of vascular structures. Herein we propose to build on this approach by using a new bio-degradable compound with pro-angiogenic properties derived from a marine diatom, i.e. shortened poly-n-acetyl-glucosamine (sNAG) nanofibers, as a scaffold for optimizing the assembly of vascular spheroids. While sNAG nanofibers are known to improve a) EC mobilization, b) angiogenesis/vascular assembly, and c) elaboration of elastin and other ECM components that provide strength and elasticity to the vessel wall in vivo and in ECs in vitro, the use of sNAG nanofibers to improve modular tissue engineering approaches has not been studied.

Hypothesis: sNAG nanofibers can be utilized for optimizing vascular spheroid assembly and therefore the functionality of bioengineered or ischemic tissues.

Rational: Engraftment and survival of transplanted vascular cells in the microenvironment of host tissues may be improved by combining such cells with biodegradable matrices to delay apoptosis and enhance regenerative properties.

Specific Aim-1: Determine the effects of sNAG nanofibers on UCB-EPC assembly and function *in-vitro:* Although EPCs have shown great potential as cell-based therapies for treatment of ischemic tissues, the development of advanced and novel biomaterials to direct the differentiation and assembly of these cells has yet to be realized. A promising strategy requires the modification of natural or synthetic surfaces to mimic endogenous proteins of the ECM. Previous studies have demonstrated that ECs will adhere to pseudo ECM structures which in turn induce intracellular signaling cascades that are able to direct cell behavior. The associated signaling interactions have the potential to promote survival of transplanted cells by induction of cell-specific adhesion to the matrix and, once attached, by controlling the proliferation, differentiation, and assembly of these vascular cells. Therefore, the first aim will test sNAG stimulated UCB-EPCs for their ability to differentiate into functional ECs, and whether they assemble into a cohesive endothelium and form cell-cell junctions. *The hypothesis for this aim is that sNAG nanofiber topographies will provide an optimal or instructive interface for inducing UCB-*

EPC differentiation towards the EC lineage and will enhance the assembly of UCB-EPCs into a cohesive endothelium.

Specific Aim-2: Determine the effects of sNAG nanofibers on UCB-EPC:ADSC-VSMC:AoAF co-assembly and maturation of vascular networks *in-vitro:* While delivery of EPCs has been shown to be successful in promoting new capillary formation in vivo and in vitro, the structure of the newly formed vessels is often non-ideal. The vessels can be immature, leaky, and lack essential cellular and extracellular components required for proper function. Immature vascular structures may result in poor blood perfusion and possibly vessel regression upon a decrease in the vascular stimulus. In addition, the formation of small capillaries alone is not likely to be sufficient for vascularization of large, complex tissues, which are often required for bioengineering strategies. Thus, the second aim is focused not only on the initial assembly of vascular networks, but on the expansion and stabilization of neovessels, which means the formation of mature, long-lasting structures. We will test whether sNAG nanofibers induce physiologic alignment and organization of vascular cell types, whether sNAG nanofibers facilitate recruitment of mural cells to nascent vascular structures, and whether sNAG nanofibers augment vessel stabilization via synthesis and deposition of basement membrane proteins. *The hypothesis of this aim is that sNAG nanofibers will enhance heterotypic interactions between vascular cell types which will result in the formation of a mature and stabilized vascular network.*

CHAPTER 3: METHODS AND MATERIALS

1. Engineering of pGlcNAc (sNAG) Nanofiber Substrates:

Native diatom-derived pGlcNAc (Marine Polymer Technologies, Inc. Danvers, MA, USA) fibers have average length dimensions of ~ 80 μm and a molecular weight of ~ 3,000,000 Da. Gamma radiation of NAG fibers resulted in length shortening, so that the resultant biodegradable nanofibers (sNAG) have an average length of 4 μm to 7 μm, a width of 100 nm to 150 nm, and a thickness of 40 nm to 60 nm, as previously measured by electron microscopy. After this treatment, while the molecular weight decreases to roughly 60,000 Da, the polymeric nanofibers maintain their unique 3D structure. All sNAG nanofibers are free of proteins, metal ions, and other contaminants. [41] An aqueous master-stock of 10 mg/ml sNAG nanofiber solution was kindly provided by the Muise-Helmericks lab. The two concentrations of polymer solutions studied for modular scaffolds were a) 10 μg/ml and b) 100 μg/ml.

2. Isolation, Characterization, and Culture of Cells:

2.1 UCB-EPC Isolation and Characterization: (Studies performed previously in Dr. Fan Lab)

EPCs were isolated and characterized in collaboration with Dr. Fan's lab. Briefly, unseparated cord blood will be diluted 1:4 with Hank's Balanced Saline Solution (HBSS, Gibco-BRL, Grand Island, NY, USA). Cord blood mononuclear cells were then isolated

using Ficoll density gradient centrifugation (Lymphoprep). Recovered cells were washed twice with HBSS and enumerated. They were then re-suspended in phosphate buffered saline (PBS). Uniform magnetic beads (Miletnyi Biotech, Bergish-Gladbach, Germany) coated with a monoclonal antibody specific for human CD34 was then used to separate out CD34+ cells. These cells were then re-suspended in 300 µl PBS, 5 mM EDTA. They were then incubated with beads (ratio 100 µl beads per 10^8 cells) for 15 minutes at 4C and processed through a MACS separation column to obtain purified CD34+ cells.

For identification of EPCs, the purified mononuclear cells were incubated with FTIC-labeled anti-KDR (Sigma Chemical Co. St. Louis, MO, USA), anti-AC133-PE (Miltenyi Biotech), anti-CD31 (Pharmigen, San Diego, CA, USA), and anti-CD34 (Becton-Dicklinson, San Jose, CA, USA) antibody. The percentage of positive cells were then analyzed by two-color flow cytometry (FACScan, Becton Dicklinson) and compared to an IgG isotype control.

All procedures for collecting human tissue (umbilical cord EPCs) were approved by the Medical University of South Carolina Institutional Review Board.

2.2 Directed Differentiation of Human ADSCs to the VSMC-lineage In-vitro: (Studies performed previously in Dr. Visconti Lab)

To investigate the SMC-potential of ADSCs, we developed an ex vivo differentiation protocol that directs the smooth muscle differentiation of hADSCs without introduction of transgenes or exposure to reagents that non-specifically alter

DNA (e.g., 5-azacytadine). To accomplish this, we modified the protocol described by Ross et al. [46] who differentiated MAPCs to the VSMC lineage: ADSCs (CD29+, CD44+, CD73+, CD90+, CD105+, CD166+; CD14-, CD31-, CD45-, Lin1-; (Lonza) are plated at 2.0 x 10^5 cells/cm^2 on tissue culture plastic in serum-free ADSC medium supplemented with 5.0 ng/ml TGF-b1 (R&D Systems, Minneapolis, MN, USA) with medium changes every 2 days. After 6 days in differentiation medium, cells are moved to expansion medium (ADSC medium supplemented with 5% fetal bovine serum (FBS) (Invitrogen, Carlsbad, CA, USA), and 5.0 ng/ml TGF-b1 (R&D Systems, Minneapolis, MN, USA) Cells were passaged every 6 days using using Trypsin/EDTA (0.025% Trypsin and 0.01% EDTA) (Cascade Biologics, Eugene, OR, USA)

2.3 In-vitro Expansion of Cells:

Human microvascular endothelial cells - cardiac (hMVECs-C) and human aortic adventitial fibroblasts (AoAFs) were purchased from Lonza. hADSCs were also purchased commercially from Lonza. Cells were cultured in 75cm^2 culture flasks (VWR, Bridgeport, NJ, USA) in 37C, 5% CO2 humidified incubators. HMVECs-C and UCB-EPCs were cultured in EGM-2 media (Lonza): Endothelial basal medium-2 supplemented with EGM SingleQuots containing hydrocortisone, 2% fetal bovine serum (FBS), human fibroblast growth factor-b (hFGF-B), vascular endothelial growth factor (VEGF), insulin-like growth factor-1 (IGF-1), ascorbic acid, heparin, human epidermal growth factor (hEGF), and GA-100 (gentamicin, amphotericin-B). ADSC-VSMCs were cultured in expansion medium as previously described (serum-free ADSC-medium, 5% FBS, 5.0%

TGF-b1). AoAF were cultured in stromal cell basal media (SCGM), (Lonza) supplemented with SingleQuot growth factors: (hFGF-B, insulin, 10% FBS, GA-1000). AoAFs, hMVEC-Cs, and UCB-EPCs were passaged (P3-P8) using Trypsin/EDTA solution (Cascade Biologics) and harvested when 80% confluent. ADSC-VSMCs were passaged (P3-P6) using Trypsin/EDTA solution (Cascade Biologics) and harvested at 90% confluency.

3. Biofabrication of Vascular Microtissue Spheroids

3.1 Casting of Micro-molded Non-adhesive Hydrogels:

Non-adherent gels for gravity-enforced spheroid assembly were casted using Microtissues 3D Petri Dish™ 24-35 Large Spheroids molds (MicroTissues Inc., Sharon, MA, USA). Briefly, a suspension of 2% w/v agarose (Fisher Scientific. Waltham, MA, USA) in sterile 0.9% NaCl was prepared and subsequently heated in the microwave. Using aseptic technique, 330 µl of molten hot agarose was pipetted into a 24-series micro-mold (35 hemispheric circular recesses, 400 µm diameter 800 µm deep in a 5 x 7 array). After the agarose was cooled, the molds were removed by gently flexing the rubber platform. When the gelled agarose was removed from the micro-mold, it was then transferred to a standard 24-well tissue culture dish (Fischer Scientific). The wells were filled with cell culture medium (EGM-2 for homotypic cell culture and serum-free ADSC-medium supplemented with 5.0% TGF-b1 for heterotypic cell culture) and incubated for 30 min at 37C for equilibration of the agarose gel. Culture medium was aspirated prior to experimentation.

3.2 Assembly of Microtissue Spheroids in the Micro-molded Recessions:

Microtissue spheroids were generated using Microtissues 3D Petri Dish™24-35 Large Spheroids (MicroTissues Inc.) molds according to established procedures. Cells were trypsinzed, counted, and re-suspended to the desired cell density (280,000 cells/75 µl; approximately 8,000 cells/spheroid). Prior to seeding, homotypic (UCB-EPCs and hMVECs-C only) cultures were re-suspended in EGM-2 media and treated with VEGF 50 ng/ml, sNAG 10 µg/ml, or sNAG 100 µg/ml. For heterotypic (UCB-EPC:ADSC-VSMC:AoAF) cultures, cells were re-suspended in serum-free ADSC-medium supplemented with 5.0 nm/ml TGF-b1 and treated with VEGF 50 ng/ml, sNAG 10 µg/ml, or sNAG 100 µg/ml. For heterotypic cell suspensions, ratios of cell types consisting of 3:1:2 were used such that the total seeding density was held constant (e.g. 280,000 cells/75 µl; approximately 8,000 cells/spheroid). Cell suspensions were then added dropwise via micropipette to the center of the rectangular recess seeding chamber of each gel. Initial settling of cells was facilitated by manual agitation and swirling of culture plates to ensure homogenous distribution into the hemispheric circular recesses. Cells were allowed to settle for approximately 10 min before additional corresponding medium was added to the cell culture plate by pipetting into the media exchange ports (1.0 ml/well for a 24-well plate). Cultures were fully immersed in their respective culture media, which were maintained in a 37C, 5% CO2 humidified incubator for 24 or 72 hours. Media and supplemental factors were refreshed daily for the duration of culture.

3.3 Whole-mount Fixation of Microtissue Spheroids:

Microtissues were washed three times in phosphate-buffered saline (PBS; 150 mM NaCl, 6.5 mM Na2HPO4-2H2O, 2.7 mM KCL, 1.5 mM KH2PO4, pH 7.4; (Sigma Chemicals Co) and fixed for 30 min in 4% paraformaldehyde (Sigma Chemicals). Following fixation, microtissue spheroids were rinsed thoroughly in PBS supplemented with sodium azide (PBSA; NaN3, 0.01% v/v) before undergoing permeabilization with phosphate-buffered Trition X-100 (0.1% Trition X-100/PBS + 0.01% sodium azide). Permeabilized microtissues were washed again in PBSA, followed by incubation in Background Buster (Innovex Biosciences, Richmond, CA, USA) blocking solution for 1h at room temperature on an orbital shaker. Microtissue spheroids were washed another three times in PBSA and prepared for immunolabeling.

3.4 Immunofluorescence Labeling of Microtissue Spheroids:

Primary antibodies specific for desired proteins as well as animal-matched fluorescence-labeled secondary antibodies were diluted in 3% BSA-containing Tris-buffered saline (TBS, 20 mM Tris base, 155 mM NaCl, 2 mM EGTA, 2 mM MgCl2). Immunofluorescence-based analysis of homotypic (UCB-EPCs and hMVECs-C only) microtissues required antibodies specific for mouse anti-human PECAM-1 IgG1 kappa (Abnova, Taipei, Taiwan; diluted 1:100). Alternatively, double and triple labeling of heterotypic (UCB-EPC:ADSC-VSMC:AoAF) microtissues required antibodies specific for mouse anti-human PECAM-1 IgG1 kappa (Abnova; diluted 1:100), goat anti-human aSMA IgG (Abcam, Cambridge, MA, USA; diluted 1:200), rabbit anti-human HSP-47 IgG

(Abcam; diluted 1:150), rabbit anti-human collagen-I IgG (Cedarlane, Burlington, NC, USA; diluted 1:200), and rabbit anti-human collagen-IV IgG (Cedarlane; diluted 1:200). Primary antibodies were visualized using animal-matched secondary antibodies including: Cy3-coupled anti-mouse (Sigma Aldrich; diluted 7:1000), Cy5-coupled anti-goat (Jackson ImmunoResearch; diluted 7:1000), and FITC-coupled anti-rabbit secondary antibodies (Sigma-Aldrich; diluted 7:1000). Primary and secondary antibodies were sequentially incubated with microtissue spheroids for 24 hours at 4C with three PBSA washings in between. Counterstain with Hoechst 33353 for 24 hours at 4C (Molecular Probes, Eugene, OR, USA; diluted 1:10,000) was used to visualize cell nuclei. After rinsing at room temperature in PBSA, samples were mounted whole onto concave glass slides (Fisher Scientific) to prevent destruction of the 3D microtissue structure. Coverslips were mounted onto microscope slides using Fluoro-Gel (Electron Microscopy Sciences, Hatfield, PA, USA) as a mounting medium and sealed using nail enamel.

3.5 Fluorescence-based Characterization of Microtissue Spheroid Morphologies by Confocal Microscopy:

After immunolabeling, the cellular organization of the microtissue spheroids was visualized using a Leica TCS SP5 AOBS multiphoton confocal microscope system (Leica Microsystems, Inc., Exton, PA, USA). Images were taken in sequential multichannel mode using the same confocal microscope settings for objective, gain, and offset, all optimized to prevent fluorescence signal cross-over. Lasers including: Ar-Ion gas laser 488 nm (FITC), HeNe 543 nm (Cy-3), and 633nm (Cy-5) were used to illuminate samples.

Short wavelength excitation was used for UV dyes, such as Hoechst 33353. Using 63x and 40x (total magnification 630x and 400x) oil immersion objectives, Z-stack images were generated by using the system-optimized setting for scanning microtissue sections. Digital images were obtained in TIF format and then processed for digital segmentation. Individual images of a Z-stack were then merged using ImageJ software (NIH ImageJ, National Institute of Health, Bethesda, MD, USA), to generate 3D projections. Image stacks and subsets are presented as maximum projection images of 5-stack 2D composites.

The methods described above were used to qualitatively observe the presence of newly formed vascular networks and to identify changes in ECM deposition and organization as a result of interactions between vascular cell types. Identification of these changes was visualized by focusing the microscopes field of view on either the apex surface of the spheroid or at its cross-section. Consistency in this approach was maintained by predetermining the peak immunofluorescent intensity of the control group, and then using those parameters as a baseline for comparison to the other experimental groups. Between 3 and 7 replicates were performed for each experimental condition and representative images from each group were chosen.

4. *In-Vitro* Tube Formation Assay

4.2.1 Matrigel Assay

Growth factor-reduced and phenol red free Matrigel Basement Membrane Matrix (BD Biosciences, San Diego, CA, USA) was used as a substrate for tube formation assays to determine the functional ability of the isolated vascular cells to form networks. In these studies, 200 µl of Matrigel (10mg/ml) was spread at the bottom of Lab-Tek II chamber slides (NUNC, Roskilda, Denmark) and used as a coat upon which cells were seeded. Prior to seeding, UCB-EPC cultures were re-suspended (50,000 cells/200 µl per well) in EGM-2 media and treated with VEGF 50 ng/ml, sNAG 10 µg/ml, or sNAG 100 µg/ml. Experimentation with passage matched (P6) hMVECs-C were used in parallel in this assay under identical culture conditions. For heterotypic (UCB-EPC:ADSC-VSMC:AoAF) cultures, cells were re-suspended in serum-free ADSC-medium supplemented with 5.0 ng/ml TGF-b1 and also treated with VEGF 50 ng/ml, sNAG 10 µg/ml, or sNAG 100 µg/ml. The ratios of cell types consisting of 3:1:2 were used such that the total seeding density was held constant (e.g. 50,000/200 µl per well). Cultures were incubated in a humidified incubator at 37C with 5% CO2 for 7 and 24 hours.

4.2.2 Imaging and Analysis of Matrigel Assay

Following formation of vascular networks, cultures were fixed in 4% paraformaldehyde (Sigma Chemical Co) for 30 min and then washed multiple times with PBSA. The initial assembly (7-hour) or regression (24-hour) of vascular networks was

visualized using a Leica DMIL inverted light microscope (Leica Microsystems). Phase-contrast images (20 random fields/well) were acquired at 20x (total magnification of 200x) to determine the number of sprouting and branching points of the newly formed vascular networks. The average number of branches and sprouts per high-powered field were counted manually using imageJ software to form each n-number from each well. Results represent the mean branching and sprouting points from at least two different experiments performed in duplicate.

4.3.1 Modified Matrigel Assay

To visualize the ability of ADSC-derived VSMCs to migrate toward and contribute to the mural cell population around a nascent endothelial cell network, heterotypic cell cultures were immunolabeled for proteins of interest. However, in order to produce gels that were thin enough for successful confocal imaging, the standard protocol was slightly modified. In brief, growth factor-reduced Matrigel (100 µl rather than 200 µl as previously described) was thawed on ice overnight and spread evenly over each well of Lab-Tek II chamber slide (NUNC). Plates were incubated for 30 min at 37C to allow for polymerization of gels. Once solidified, serum-free ADSC-medium supplemented with 5.0 ng/ml TGFb-1 was added for 1 hour at 37C to equilibrate the matrices. Approximately 5.0x 10^4 UCB-EPCs, ADSC-derived VSMCs, and AoAFs (3:1:2 ratio) were plated in individual wells and incubated in a humid atmosphere at 37C in 5% CO2. After 7-hours, cultures were fixed overnight in 4C with 2% (w/v) pipes-buffered paraformaldehyde (Sigma Chemical Co).

4.3.2 Immunofluorescence Labeling of Tube-like Networks

The cellular components of the vascular structures were characterized via immunolabeling with mouse anti-human PECAM-1 IgG1 kappa (Abnova; diluted 1:100) as an endothelial cell marker, goat anti-human aSMA IgG (Abcam; diluted 1:200) as a pericyte marker, and rabbit anti-human HSP47 IgG (Abcam; diluted 1:150) as an ECM marker. Primary antibodies were conjugated with coordinate secondary antibodies as described previously; Cy3-coupled anti-mouse (Sigma Aldrich; diluted 7:1000), Cy5-coupled anti-goat (Jackson ImmunoResearch; diluted 7:1000), and FITC-coupled anti-rabbit secondary antibodies (Sigma-Aldrich; diluted 7:1000). Counterstain was achieved using Hoechst 33342 (Molecular Probes: diluted 1:10,000) to visualize cell nuclei. Samples were washed three times and maintained in PBSA at 4C until slides were ready to be removed from the chamber. Coverslips were mounted onto slides using Fluoro-Gel (Electron Microscopy Sciences) as a mounting medium and sealed using nail enamel.

4.3.3 Fluorescence-based Characterization of Tube-like Network Formation by Confocal Microscopy:

After immunolabeling, vascular network formation was visualized using a Leica TCS SP5 AOBS multiphoton confocal microscope system (Leica Microsystems). Images were taken in sequential multichannel mode using the same confocal microscope settings for objective, gain, and offset, all optimized to prevent fluorescence signal cross-over. Lasers including: Ar-Ion gas laser 488 nm (FITC), HeNe 543 nm (Cy-3), and 633nm (Cy-5) were used to illuminate samples. Short wavelength excitation was used

for UV dyes, such as Hoechst 33353. Using 63x (total magnification 630x) oil immersion objective, Z-stack images were generated by using the system-optimized setting for scanning matrigel sections. Digital images were obtained in TIF format and then processed for digital segmentation. Individual images of a Z-stack were then merged using ImageJ software (NIH ImageJ) to generate 3D projections. Image stacks and subsets are presented as maximum projection images of 5-stack 2D composites.

5. Statistics:

Statistical analysis including calculations of standard error of means and mean comparisons (Students t-test) were performed using Prism (Version 5.0, Graphpad Software, La Jolla, CA) P-values greater than 0.05 were determined to be statistically significant.

CHAPTER 4: RESULTS

1. Cell Culture and Spheroid Formation

Figure 1: ***Human EPC Isolation, Culture, and Characterization (Studies performed previously in Dr. Fan Lab).*** In previous studies performed by Dr. Fan, EPCs were isolated from cord blood from healthy pregnant women. Blood was diluted with HBSS (hank's balanced salt solution) followed by ficoll density gradient centrifugation. Mononuclear cells were collected and cultured in a collagen coated dish. Previous studies have shown that culture in a collagen coated dish would result in late EPCs, which have function to form tubes. After several days (7-14 days) of culture, the cells form colonies, suggesting EPCs were cultured. Dr. Fan's group then characterized the cultured EPCs using flow cytometry analysis and show that cells are positive for CD34 and VEGFR2. Fluorescence microscopy analysis indicated that cells were positively stained by Dil-acLDL and FITC-labeled lectin. When they cultured the cells in Matrigel matrix, they were able to form tubes. All these characterizations suggest that they had successfully cultured human EPCs.

Figure 2: ***Directed Differentiation of Human Adipose-derived Stem Cells to the Vascular Smooth Muscle Cell Lineage In vitro (Studies performed previously in Dr. Visconti Lab).*** To examine VSMC characteristics of ADSC-derived VSMCs, previous members of the Visconti lab performed RT-PCR and immunoblot analyses. ADSC-derived VSMCs were compared to ADSCs maintained in simple expansion medium (DMEM-LG Invitrogen, supplemented with Pen/Strep/glut and 10% FBS). As seen in **figure 5:A. B** both

transcript and protein for early markers of VSMC differentiation (aSMA and SM22) are detected first and their levels of expression increase over time. Late VSMC markers (Calponin and SM-MHC) are detected later and in increasing amounts in differentiated cell populations. Importantly, this temporo-specific and increased expression of SMC markers is similar to that exhibited by differentiating smooth muscle cells in vivo. To further support their RT-PCR and immunoblot analyses, they performed immunofluorescent microscopy of these VSMC markers. As seen in **Figure 5: C,** a limited number of ADSCs express early VSMC differentiation markers (aSMA, SM22) and no detectable late differentiation markers. As time in differentiation culture increases, expression of early markers increases and late markers are detected and also increase over time.

Figure 3: ***Microtissue Spheroid Fabrication and Processing.*** Microtissue spheroids were generated using Microtissues 3D Petri Dish™24-35 Large Spheroids (MicroTissues Inc.) molds. Molds contained 35 hemispheric circular recesses with dimensions of 400 µm diameters by 800 µm depths in a 5 x 7 array. Agarose was gelled around the micromold, and on removal, the gel contained an array of recesses complementary to the mold **(Figure 3: A-D)**. A single cell suspension of early UCB-EPCs, late UCB-EPCs, and hMVECs-C were then seeded into the cell seeding chamber of the mold. The cells sank into the recesses within 1 hour and formed a single spheroid (8,000 cells/spheroid) of uniform size in the bottom of each recess within 24 hours. Bright field microscopy revealed the successfully fabricated 300um diameter microtissues. **(Figure 3: E)**

Figure 4: ***EC Subculture and Comparison of Early-outgrowth UCB-EPCs, Late-outgrowth UCB-EPCs, and hMVEC-Cs.*** Early UCB-EPCs, late UCB-EPCs, and adult hMVECs-C are commonly studied in vascular engineering and regenerative medicine applications. Thus, understanding inherent differences between these cell types can yield important advancements in vascular regenerative medicine. To evaluate these differences, we examined general EC surface marker expression of cell adhesion molecule hPECAM-1. Using immunofluorescence analysis, we found that early UCB-EPCs had minimal expression of the endothelial cell-specific marker hPECAM-1. In contrast, late UCB-EPCs and hMVEC-Cs show profuse expression with a comparable distribution pattern of hPECAM-1 cell labeling. This result confirms that late UCB-EPCs phenotype was similar to that of mature hMVEC-Cs when sub-cultured in microtissue spheroids.

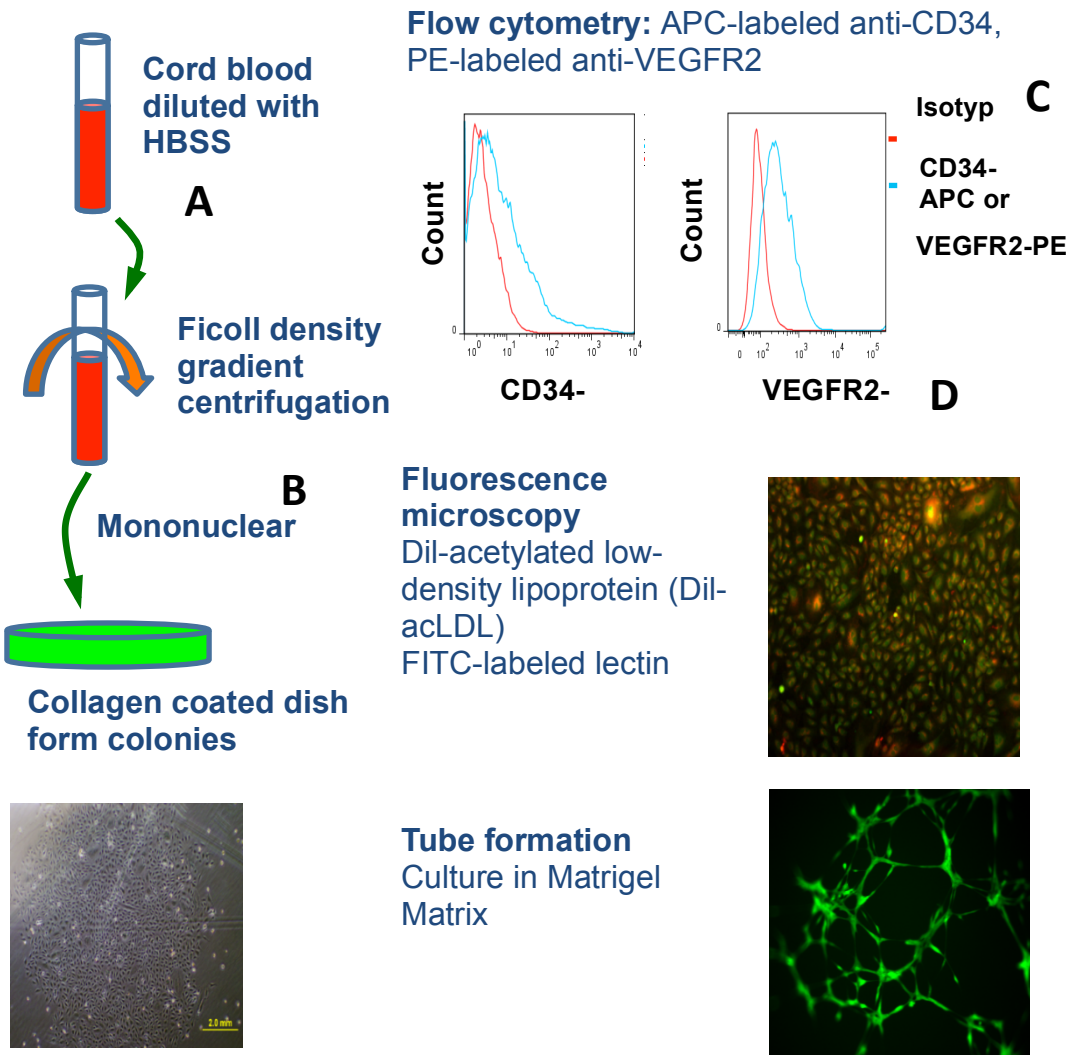

Figure 1: Human umbilical cord blood derived endothelial progenitor cell isolation, culture, and characterization *(Studies performed previously in Dr. Fan's lab)*. (a) Cord blood mononuclear cells were isolated using Ficoll density gradient centrifugation. (b) Uniform magnetic beads coated with monocloncal antibody specific for human CD34 was used to separate out CD34+ cells and processed through a MACS separation column. (c) Cells were identified using FITC-labeled anti-KDR, anti-AC133-PE, anti CD31, and anti-CD34 antibodies and analyzed using two-color flow cytometry. (d) Functional assessment was carried out using Dil-acLDL uptake and Matrigel tube formation assay.

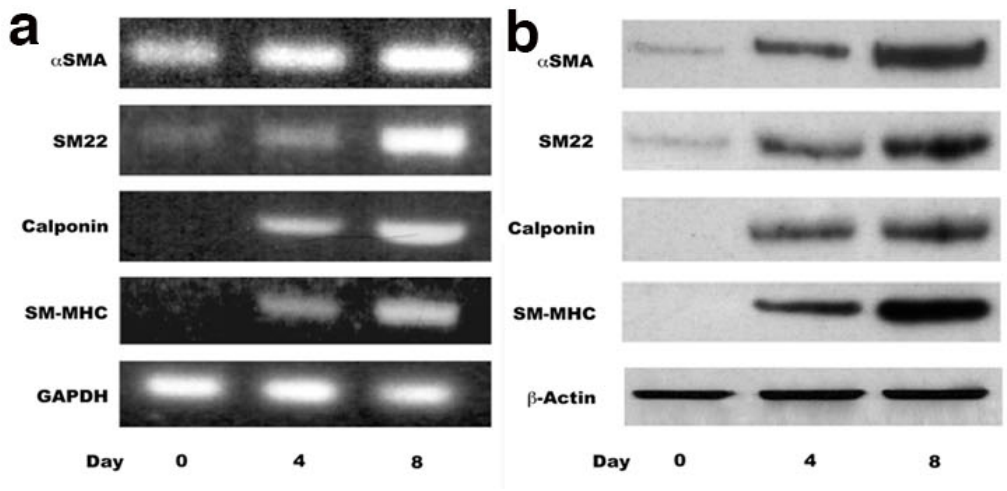

Figure 2: Directed differentiation of human ADSCs to the VSMC-lineage *in vitro* *(Studies performed previously in Dr. Visconti lab).* (a) RT-PCR analysis of smooth muscle differentiation in differentiated ADSCs at 0, 4 and 8 days in differentiation medium. (b) Immunoblot analysis of protein extracts of ADSC derived cells at 0, 4 and 8 days in diff. medium. **α**SMA = a-smooth muscle actin, SM-MHC = smooth muscle myosin heavy chain; GAPDH = glyceraldehyde 3-phosphate dehydrogenase.

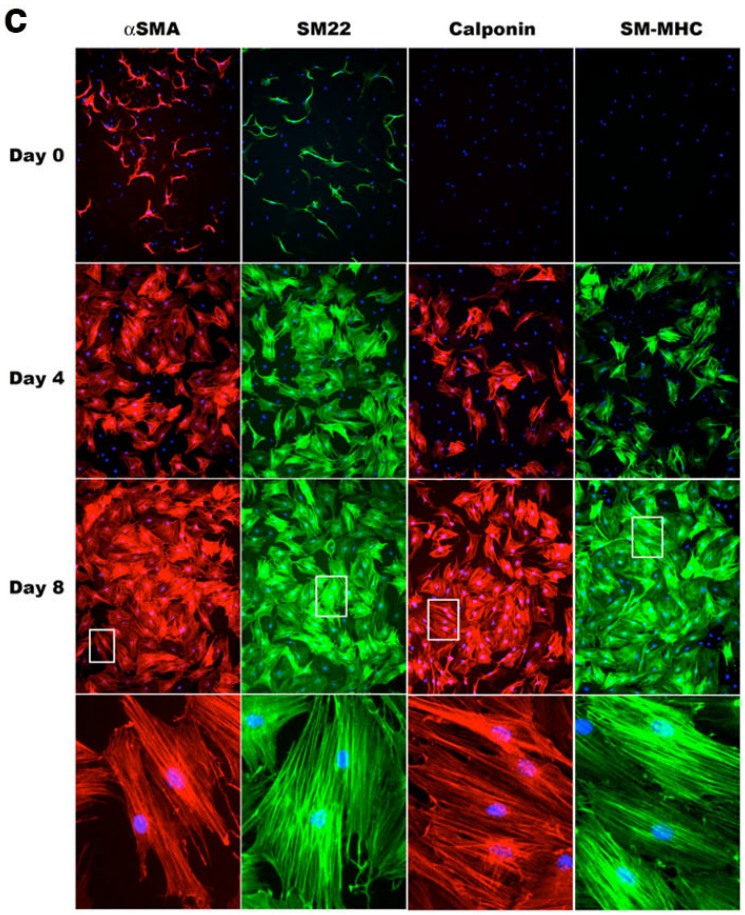

Figure 3: Directed differentiation of human ADSCs to the VSMC-lineage *in vitro* continued *(Studies performed previously in Dr. Visconti lab).* Immunofluorescence analysis of ADSC derived SMCs at 0, 4 and 8 days in diff. medium. Limited **α**SMA- and SM-22- positive cells were detected early upon addition of differentiation medium while no cells were immunopositive for the later markers of SMC differentiation (calponin and SM-MHC). By 4 days in diff. medium, **α**SMA- and SM-22-positive cells were detected at markedly higher levels and calponin- and SM-MHCpositive cells were detected. By 8 days in diff. medium, the majority of cells positive for **α**SMA and SM-22 and calponin- and SM-MHC-positive cells were observed at increased levels. Mag. = 400X.

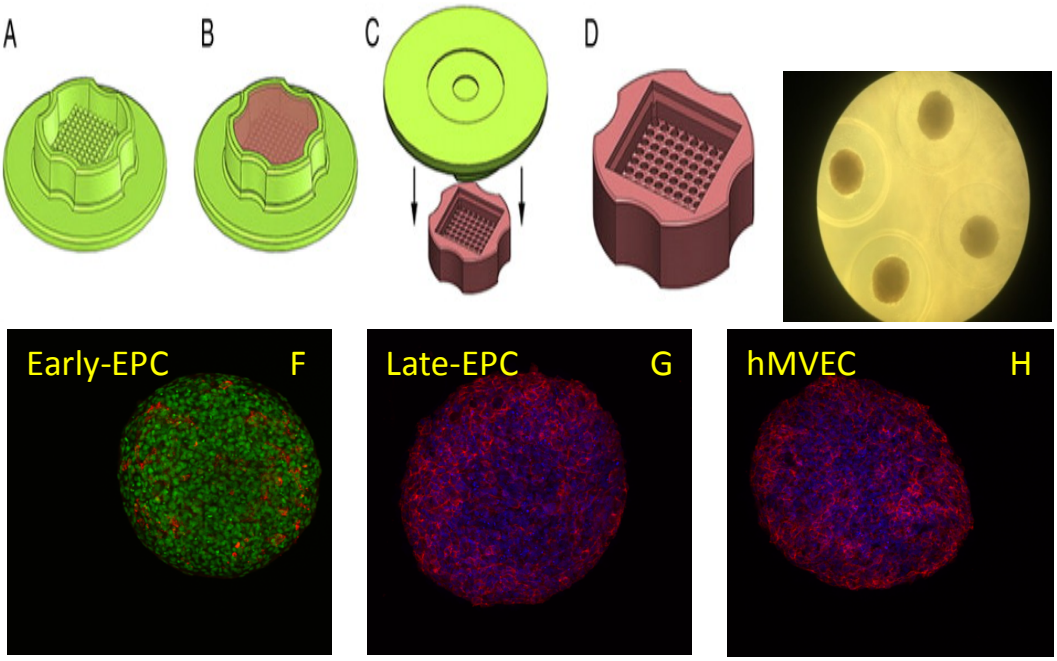

Figure 4: Fabrication of microtissue spheroids and sub-culture optimization: (a-d) Fabrication of microtissue molds for vascular spheroid formation. (e) Assembling of microtissues (EPCs) within the agarose of 3D micro-Petri dish (273,000 cells/dish) (4x). (f-h) A representative image (20x) of early-EPC, late-EPC, and hMVEC-C containing 8,000 cells/spheroid. (blue Hoescht, red hPECAM1).

2. **Specific Aim-1: Determine the effects of sNAG nanofibers on UCB-EPC assembly and function *in vitro.***

Figure 5: ***sNAG Nanofibers Induce UCB-EPC and hMVEC-C Assembly and Cell-Cell Junction Formation.*** Previous studies have demonstrated that cell adhesion molecule PECAM-1 expressed by ECs is crucial for vessel formation and maintenance. Therefore, the effect of sNAG nanofibers on UCB-EPC and hMVEC-C monoculture spheroids was investigated by confocal microscopy. Treatment with sNAG 10ug/ml **(Figure: A, B)** elicited profound effects on the organization and alignment of ECs. Our results further show that hPECAM-1 positive cells (red) aligned circumferentially around the perimeter of the spheroid, as well as along an inner core, in our sNAG 10ug/ml treated cultures. Spheroids treated with sNAG 100ug/ml demonstrated preferential hPECAM-1 localization to the periphery of the spheroid as well as increased expression around what appears to be anastomosing ECs (white arrows). Analysis of immunofluorescent images acquired from (control) 50 ng/ml VEGF-treated spheroids show that ECs circumscribed a single large central area that did not display immunoreactivity of hPECAM1 **(Figure: A, B)**

Figure 6: ***sNAG Nanofibers Effect UCB-EPC Migration and EC Differentiation.*** To determine whether sNAG nanofiber matrices induce EC migration within our spheroid system, cross-sections of spheroids were analyzed. The expression of surface adhesion

protein characteristically expressed by endothelial cells was evaluated by immofluorescence microscopy (hPECAM-1; red). Cross-sections of monoculture spheroids show localization of hPECAM-1 to the outer perimeter of the spheroids **(Figure 7: A, B)**. In sNAG 100 ug/ml and control spheroids, immunofluorescence analysis revealed a dense expression pattern at the periphery of the microtissues, a pattern that was not observed in the 50ng/ml VEGF or 10ug/ml sNAG spheroids. In 50 ng/ml and 10ug/ml spheroids, hPECAM-1 was expressed more evenly and clearly resembling a singular lumenized periphery with well-established cell-cell junctions. **(Figure 7: A, B)**. Results of this study show that sNAG 10ug/ml treated spheroids provide an optimal substrate for EC migration (a key step in EC morphogenesis and tube remodeling) using a less concentration of sNAG nanofibers.

Figure 7: ***Effect of sNAG Nanofibers on EC Function on 2D Substrates***

Late outgrowth EPCs spontaneously formed capillaries when plated on three-dimensional Matrigel extracellular matrix. At 7hr, tube structures began to form (fig. 5a). After 24 hours, the cells coalesced and formed more discrete tubes (fig 5b). Vessel sprouting was significantly higher in sNAG 10ug/ml treated spheroids and vessel branching in 100ug/ml sNAG treated spheroids. However, there were no significant differences between other treatment groups were observed, indicating that kinetics of the vasculogenesis properties of the cell types in Matrigel are effected by sNAG nanofiber treatment.

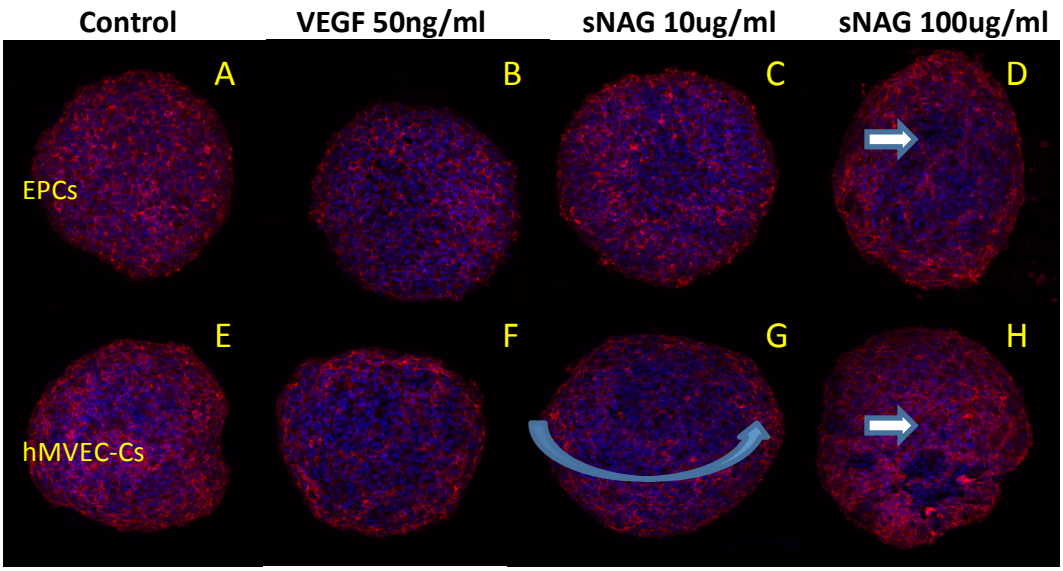

Figure 5: sNAG nanofibers effect UCB-EPC and hMVEC-C vascular assembly *in vitro*. Representative immunofluorescent images of whole-mount monoculture spheroids labeled with antibodies directed against anti hPECAM-1 (red), and counter stained with Hoescht nuclear stain (blue). Control spheroids (a and e) or spheroids treated with 50ng/ml of VEGF (b and f), demonstrate morphologies with minimal structural alignment. Spheroids treated with 10ug/ml sNAG (c and g) show increased hPECAM-1 expression localized to the periphery of the spheroid (blue arrow). Spheroids treated with 100 ug/ml sNAG (d and h) have increased peripheral hPECAM-1 expression as well as anastomosing EC structures (white arrows).

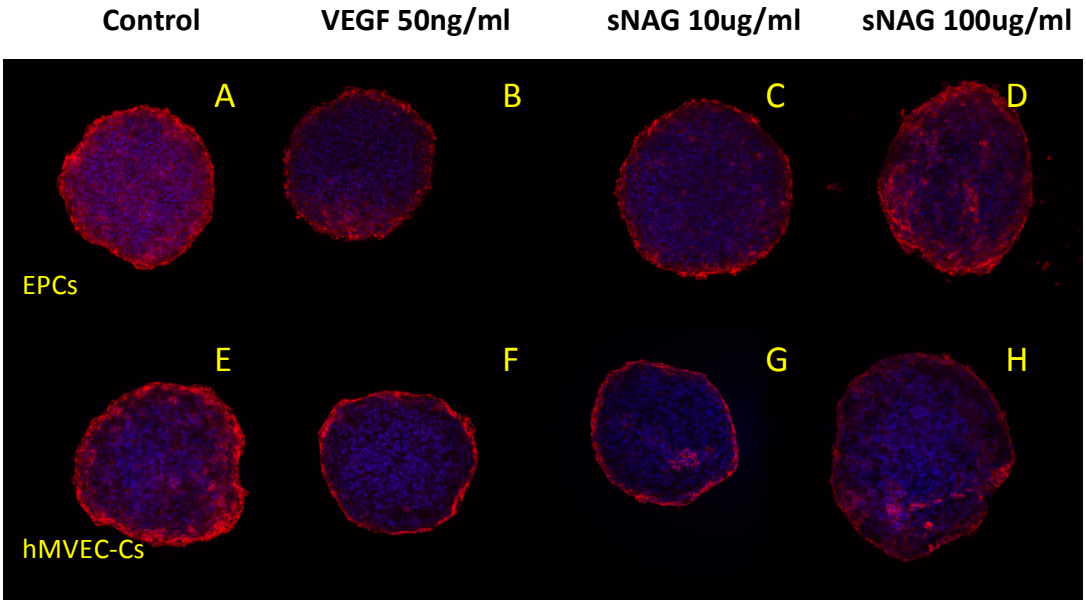

Figure 6: sNAG nanofiber matrices induce EC migration in microtissue spheroids. Representative immunofluorescent images of cross-sectioned monoculture spheroids labeled with antibodies directed against anti hPECAM-1 (red), and counter stained with Hoescht nuclear stain (blue). (a-h) Epithelialization of EC cells in spheroid culture at 1 day. (b,f and c,g) A section of a spheroid shows a peripheral monolayer of EC cells in sNAG 10ug/ml and VEGF 50ng/ml and a core of nuclei labeled cells. (a,e and d,h) Immunofluorescence dense hPECAM1 strands indicative of tight junctional cell-cell contacts in control and sNAG 100ug/ml spheroids.

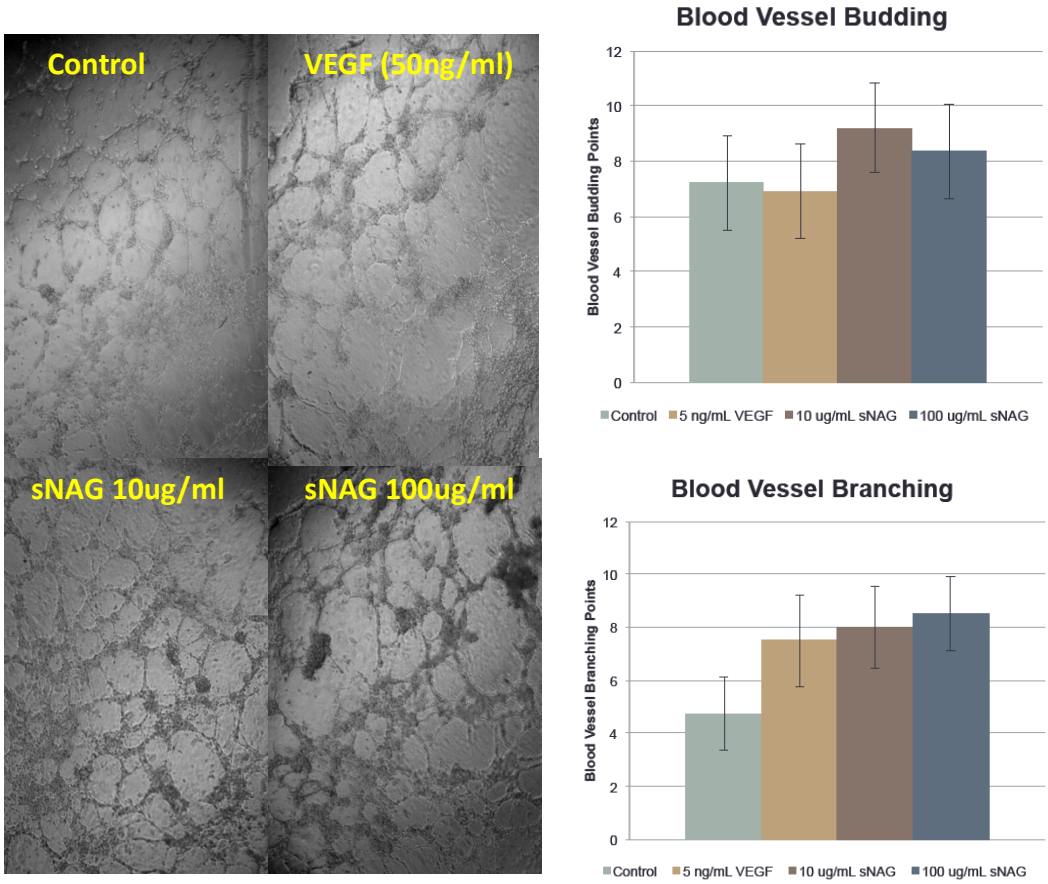

Figure 7: 2D Matrigel tube formation assay. Representative image of late-outgrowth EPCs treated with sNAG nanofibers or other known initiators of vascular assembly (VEGF 50ng/ml). sNAG 10ug/ml demonstrated a significant increase in vessel sprouting compared to VEGF 50ng/ml and control. sNAG 100ug/ml showed a strong trend in vessel branch points, although was not statistically significant compared to VEGF 50ng/ml.

SPECIFIC AIM-2: Determine the effects of sNAG nanofibers on UCB-EPC:ADSC-VSMC:AoAF co-assembly and maturation of vascular networks *in vitro.*

Figure 8: ***sNAG Nanofibers Induce Lumen Formation and Vascular-like Network Assembly.*** Cell adhesion molecule PECAM-1 expression at the cell-cell interface could be used to indicate vascularlike structures or lumina. We sought to determine the morphogenesis dynamics of UCB-EPCs treated with sNAG 10ug/ml, sNAG 100ug/ml or VEGF 50ng/ml in heterotypic cell cultures. Immunofluorescence analysis for human PECAM-1 detected EC lined vascular lumens in 100 ug/ml sNAG treated spheroids within 24 hours of cell culture **(Figure 7a)**. This process continued with lumens increasing in number and size, followed by their coalescence into larger structures **(inset)**. By day 3, vascularlike networks grew; and we could clearly observe complex and comprehensive structures within 50 ng/ml VEGF, 10 ug/ml sNAG, but most predominantly in 100 ug/ml sNAG treated spheroids. Complex vascular networks with lumenized structures were easily detected throughout the sNAG 100ug/ml treated spheroids, suggesting a mature vascular network **(Figure 7B)**. Results of this study indicate that lumen formation and vascular network assembly is increased in the sNAG 100ug/ml microtissue spheroids

Figure 9: ***Collagen Type-1 is Significantly Degraded by Day-3 sNAG Treated Microtissue Spheroids.*** To determine the contribution of structural ECM proteins, we investigated collagen type 1 deposition in sNAG treated spheroids. Significant contrast was shown

with the expression of type 1 collagen between 24h and 72h cultures treated with or without sNAG. However, reduction in type 1 collagen expression was observed across all experimental groups **(Figure 8A, B).** Results of this study show that sNAG treated microtissue spheroids undergo rapid ECM degradation by day 3 of cell culture.

Figure 10*: Induction of VSMC Expression Markers by Day-3 in sNAG Treated Microtissue Spheroids.* Given the tempero-specific degradation of Collagen type 1 by sNAG treated spheroids, we wanted to determine whether sNAG nanofibers were having an effect on the maintenance of VSMC phenotype in our ADSC-VSMC cultures. Time-course experiments revealed a time-dependent increase in aSMA expression in sNAG 10ug/ml and sNAG 100ug/ml treated cultures **(Figure 9)**. The inductive effect of sNAG nanofibers on aSMA expression could not be seen in day-1 cultures (data not shown). In contrast, 50ng/ml VEGF and control spheroids displayed diffuse aSMA expression **(Figure 9).** Notably, the expression of aSMA was located beneath hPECAM-1 staining, indicating the formation of a multi-layered cellular alignment (white arrows).

Figure 11: ***Coincident Heterotypic Cell Alignment and Collagen Type-4 Deposition in sNAG Treated Microtissue Spheroids.*** To investigate the functional characteristics of the ADSC-VSMC phenotype by sNAG nanofibers, triple immunofluorescence (aSMA, Collagen type 4, and hPECAM1) using confocal microscopy was employed. We sought to interrogate the ECM produced by EC-VSMCs by examining the spatial relationship between collagen IV, hPECAM-1, and aSMA, in cross sections of microtissue spheroids.

3-day cultures were examined for alignment of vascular cell types with associated deposition of collagen type IV proteins. Three-dimensional projections from confocal microscopy revealed that collagen IV deposited in sNAG 100ug/ml and 10ug/ml treated spheroids, but not in 50ng/ml VEGF or control microtissue spheroids. These results strongly suggest that sNAG nanofiber treated spheroids were organized into distinct vascular layers with functional properties evidenced by physiologic deposition of collagen type 4.

Figure 12: ***sNAG Nanofibers Facilitate Pericyte Recruitment to the Ablumenal Surface of EC-Lined Tubes within Vascular Guidance Tunnels.*** Next, we wanted to determine whether sNAG nanofibers enhanced the stabilization of vascular networks by enhancing recruitment of ADSC-VSMCs to the ablumenal surface of vascular networks. To do this, we first verified the EC-pericyte association of the vascular network generated by UCB-EPCs within our sNAG treated microtissue spheroids. Cross-sections of sNAG 100ug/ml treated microtissues show whole vascularlike networks covered by aSMA + pericytes (white arrows), especially on the abluminal endothelial surface, which could be confirmed through 3D images obtained by confocal microscopy **(Figure 10: white arrows).** Further analysis shows that matrix spaces (i.e., vascular guidance tunnels) are readily observed during morphogenesis that directly corresponds to the area surrounding aSMA + cells **(Figure 10: sNAG 100ug/ml, blue arrows)**. These data show that a strong synergistic relationship exists between these 2 cell types during critical extracellular remodeling events necessary for vasculogenic plexus assembly.

Basement membrane assembly on the abluminal surface of blood vessels is required to initiate the interaction between ECs and pericytes as a critical step of vessel maturation in vitro and in vivo. Thus, we explored the effect of sNAG treated heterotypic cell cultures on basement membrane assembly around nascent blood vessel networks. To determine the position of basement membrane matrix in relation to ECs, pericytes, and vascular guidance tunnels **(Figure 10)**, we stained for collagen type 4, which shows its presence between the EC and pericyte surfaces surround the vascular guidance tunnels (White arrows). Thus, under the 100ug/ml sNAG treated spheroid conditions, ECs and pericytes will co-assemble into tube structures with an associated basement membrane matrix **(Figure 10)**. Overall, our data strongly support the concept that pericyte recruitment to EC-lined tubes catalyzes extracellular deposition of basement membrane matrix components using confocal microscopy.

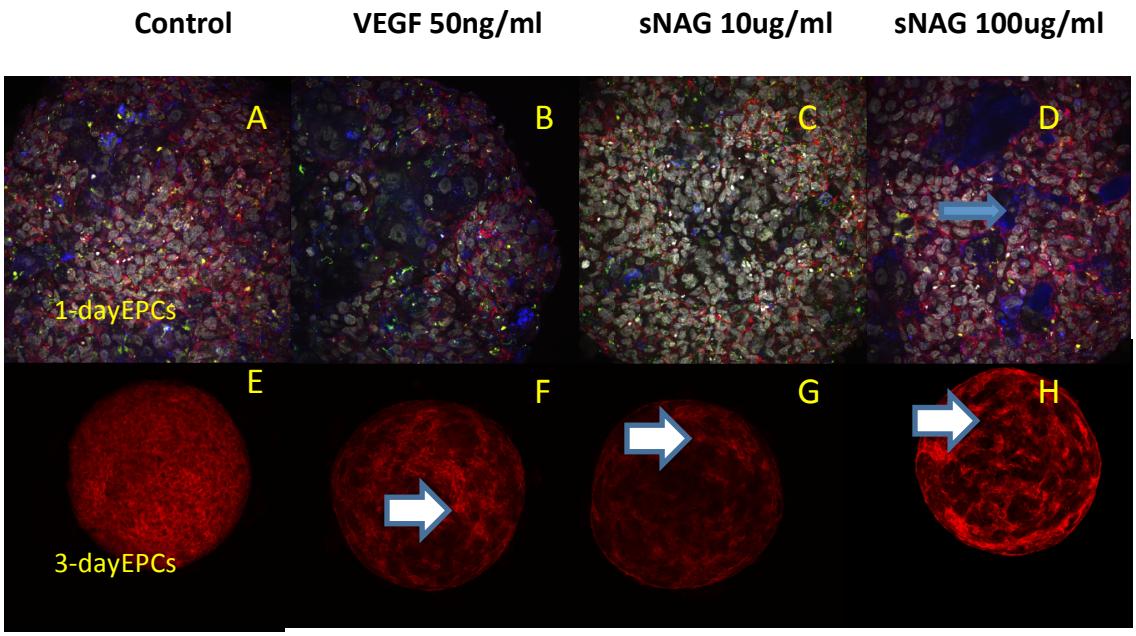

Figure 8: sNAG nanofibers induce lumen formation and vascular network assembly over time. Representative immunofluorescent images of whole-mount heterotypic spheroids ((top row 24h) and (bottom row 72 hours)) labeled with antibodies directed against anti hPECAM-1 (red). (Top row) sNAG 100ug/ml spheroids form multiple, large lumenized structures (white arrows) after 24 hrs in culture. In contrast, VEGF 50ng/ml and 10ug/ml sNAG show moderate lumen formation (blue arrow), while control spheroids were unable to form lumenized structures. (Bottom row) hPECAM-1 labeled cells show the organization of UCB-EPCs into a vascular-like network after 3 days cell culture (20x). sNAG 100ug/ml treated spheroids assembled into complex vascular networks with an organized, hierarchical organization (white arrow indicates branched and elongated vascular networks). Spheroids treated with VEGF 50ng/ml and 10ug/ml were also able to assemble into vascular networks by day 3 (white arrows). In contrast, control spheroids maintained a quiescent EC phenotype and did not undergo morphological changes.

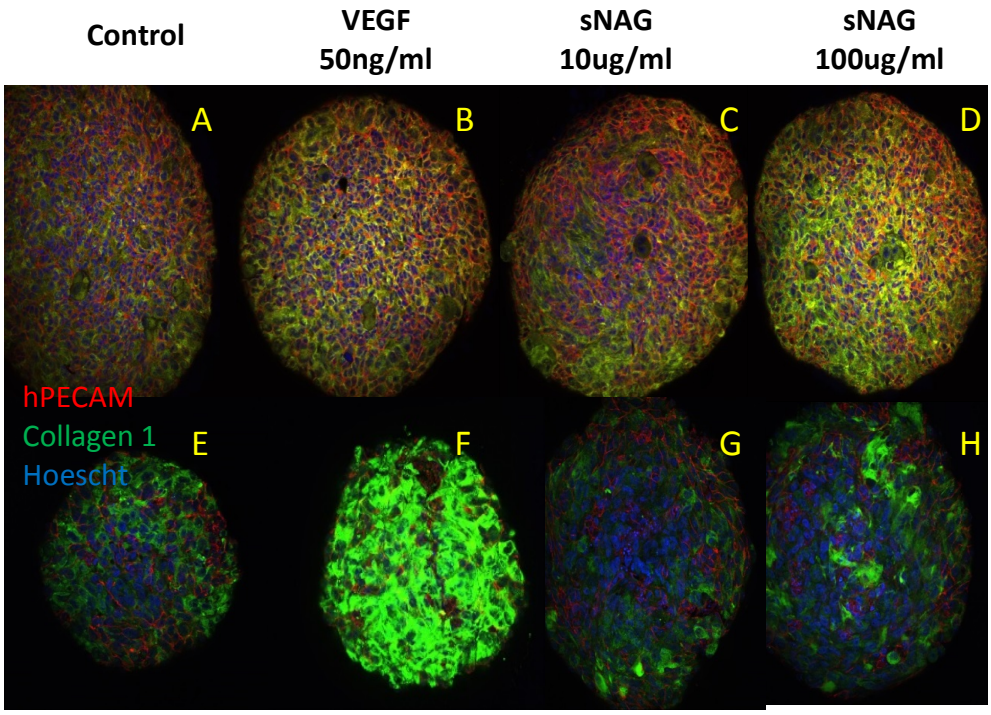

Figure 9: Collagen type 1 is reduced in sNAG treated spheroids after 3 days cell culture. sNAG nanofiber treated spheroids significantly reduce Collagen type-1 deposition after 3-days cell culture. Representative images of whole-mount heterotypic spheroids (24 and 72 hours) labeled with antibodies directed against anti-hPECAM1, anti-human collagen-1, and counterstained with Hoescht 3553 nuclear stain. (b-d) In day 1 cultures, sNAG 100ug/ml, 10ug/ml and VEGF 50ng/ml show increased collagen-1 deposition compared to control. (f) By day 3, VEGF 50ng/ml was significantly augmented compared to sNAG and control spheroids.

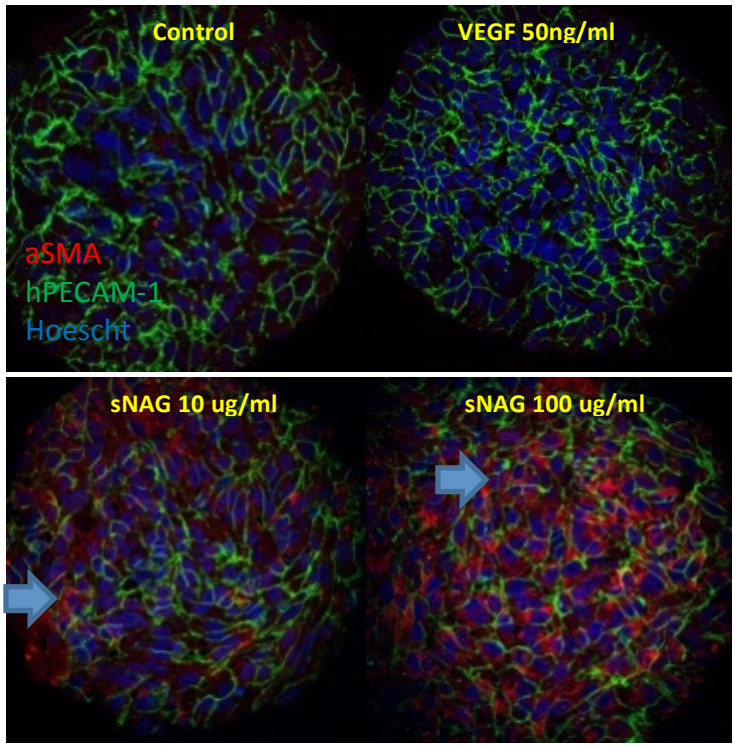

Figure 10: Induction of SMC markers by ADSCs in 3-day cell culture. Representative images of whole-mount heterotypic spheroids (72 hours) labeled with antibodies directed against anti-hPECAM1, anti-human aSMA, and counterstained with Hoescht 3553 nuclear stain. sNAG 100ug/ml spheroids show significantly increased aSMA expression compared to VEGF 50ng/ml and control. sNAG 10ug/ml also displayed increased aSMA expression, but was less abundant compared to sNAG 100ug/ml.

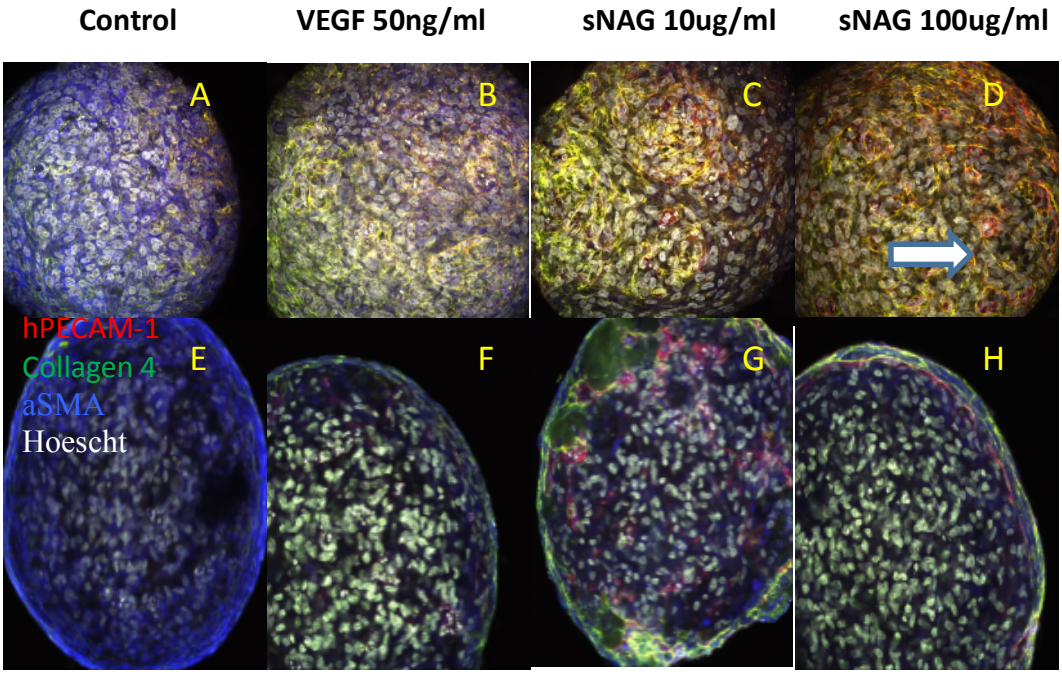

Figure 11: Heterotypic interactions during vascular spheroid formation in sNAG treated cultures increased collagen type-4 deposition. (c,d and g,h) sNAG nanofibers augment heterotypic cross-talk and alignment between UCB-EPCs and ADSC-VSMCs. Images reveal basement membrane deposition (white arrow heads) around developing microvessels in sNAG 100ug/ml treated tissues. These arrows also reveal the co-assocaition of these 2 cells at this location. (b,f) VEGF 50ng/ml treated spheroids show minimal cellular alignment with scant amounts of collagen type-4 deposition. (a, e) Control spheroids did not express collagen type-4 and show no cellular alignment or organization.

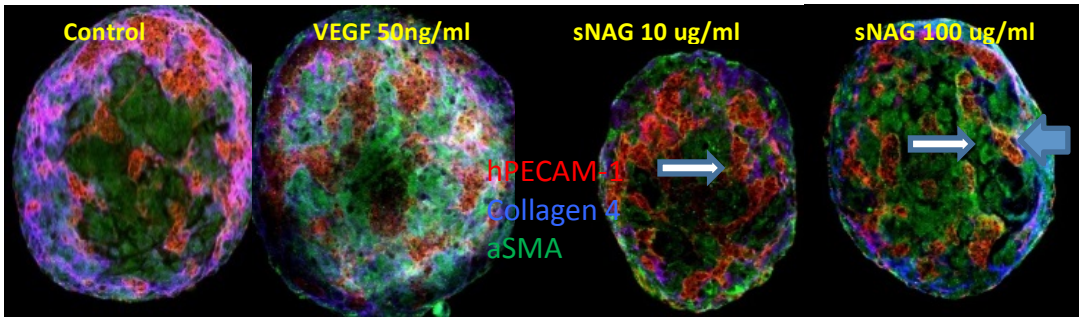

Figure 12: Recruitment of pericytes to the ablumenal surface of EC-lined tubes within vascular guidance tunnels. Heterotypic microtissue spheroids were allowed to assemble for 3 days, fixed, and processed for immunofluorescence using confocal microscopy. UCB-EPCs were stained with endothelial specific marker, hPECAM1 (red), whereas ADSC-VSMC were labeled with aSMA (green). sNAG 100ug/ml treated spheroids show association of pericytes with endothelial tubes on the abluminal surface (white arrows). ECs form a continues layer with ADSC-VSMCs recruited to the basal surface (White arrows). Blue arrows indicate the border of the vascular guidance tunnel and the entrance of ADSC-VSMCs to these boarders. Basement membrane matrices were stained with collagen IV (blue). Staining of aSMA (green) versus the col-4 (blue), reveals the location of the pericytes in relation to the baseent membrane. This reveals a continuous basement membrane (arrows) along the ablumenal surface of developing microvesssels and between the perivascular cells and the endothelium.

Chapter 5: DISCUSSION

CELL CULTURE

Adipose-derived stem cells represent a promising source of autologous post-natal stem cells that have the advantage of ease of harvest, minimal discomfort to the patient and high yield through percutaneous harvest. Like bone marrow and umbilical cord mesenchymal stem cells, ADSCs are able to differentiate into cells of mesodermal origin. Further, ADSCs can be cryopreserved then thawed without negatively impacting their viability and plasticity. Compared to ES or iPS cells, ADSCs do not require genetic reprogramming to induce pluripotency, reducing the likelihood of teratoma formation in vivo. While ADSCs do not possess the broad plasticity of either ES or iPS cells, limited mesodermal plasticity may prove more safe and suitable for differentiation of mesodermal cell populations. Several groups have reported that ADSCs can be induced to differentiate to SMCs or pericyte-like cells in vitro by cytokines or chemical agents. In the present study, we use a differentiation protocol that avoids the introduction of transgenes or non-specific reagents that may have unanticipated effects on the genome of differentiated cells, providing greater opportunity for the introduction of ADSC-derived VSMCs to *in vivo* systems.

To demonstrate that ADSCs can be committed to the VSMC lineage using our protocol, cells were grown in serum-free ADSC medium supplemented with 5.0 ng/ml TGF-b1 as previously described. After five days in our differentiation medium, ADSCs exhibited smooth muscle cell morphology, including detectable contractile fibers, while

control ADSCs did not undergo VSMC differentiation. To further examine VSMC characteristics of ADSC-derived VSMCs, RT-PCR and immunoblot analyses were performed by the Visconti lab. Results show that both transcript and protein for early markers of VSMC differentiation (aSMA and SM22) are detected first and their levels of expression increase over time. Late VSMC markers (Calponin and SM-MHC) are detected later and in increasing amounts in differentiated cell populations. Importantly, this temporo-specific and increased expression of SMC markers is similar to that exhibited by differentiating smooth muscle cells *in vivo*.

In support of previous RT-PCR and immunoblot analyses, immunofluorescent microscopic assays of these VSMC markers were also examined by the Visconti lab. Results demonstrate that a limited number of ADSCs express early VSMC differentiation markers (aSMA and SM22) while no detectable late differentiation markers were observed. As time in differentiation culture increased, expression of early markers increased and late markers are detected and also increased over time. These results suggest that as ADSCs differentiate into VSMCs, their rate of proliferation decreases compared to undifferentiated ADSCs. Collectively, these experiments provide strong evidence that ADSCs are capable of being differentiated into the VSMC lineage and may represent a suitable alternative cell source for vascular tissue engineering applications.

Another significant challenge in advancing prevascularization strategies in tissue engineering is the lack of easily isolated autologous EC sources. The ability to isolate late-outgrowth EPCs noninvasively from peripheral blood and expand the colonies in long-term cultures is a major development for autologous cell therapies. Late-

outgrowth EPCs have been pursued as an alternative cell source for tissue engineering strategies. The two to three week time interval before EPC colonies are observed is a clinical drawback for emergency interventions, but the cells are highly proliferative, capable of undergoing more than 30 population doubling while maintaining a stable EC phenotype during long-term culture, justifying their use for cellular therapies.

To establish procedures for the generation prevascularized microtissue spheroids, we employed similar techniques that have been developed for the generation of tumor cell spheroids. We seeded EC suspension into non-adherent micromolds, which led to the formation of uniform microtissue aggregates within 24 hours. The initial series of experiments we performed were to compare the phenotypic characteristics of late-outgrowth UCB-EPCs to early-outgrowth UCB-EPCs and mature hMVEC-Cs when grown under identical culture conditions in our 3D microtissue spheroid model. Panendothelial marker hPECAM-1 expression was used as a sign of EC maturation and visualized using confocal microscopy. Results show intermittent hPECAM-1 expression throughout the spheroid in early-outgrowth UCB-EPC and ECs failed to differentiate into a surface monolayer as compared to late-outgrowth UCB-EPCs and hMVEC-Cs. Next, we examined whether inherent differences in hPECAM-1 expression existed between late-outgrowth UCB-EPCs and hMVEC-Cs; and found that UCB-EPCs and hMVECs have comparable levels of hPECAM-1 expression. This is indicative of their maturation state, as these markers are typically associated with a more mature endothelial phenotype. Overall, these results suggest that UCB-EPCs were successfully differentiated into a mature EC phenotype in our optimized 3D microtissue

spheroid model and that they may be a suitable alternative cell source for tissue engineering applications.

The nanofiber method has advantages over conventional suspension culture methods for anchorage-dependent cells. As compared to conventional spheroid culture, nanofiber supplemented suspension cultures can improve spheroid formation efficiency and possibly cell viability. In contrast to microcarrier cultures, in which the shear stress could damage cells cultured on the microcarrier surface, the cells inside of the spheroids are protected from shear damage in nanofiber-supplemented suspension culture. Because the nanofiber material is poly-N-acetyl glucosamine, which are biocompatible and biodegradable, cells cultured with sNAG nanofibers can be transplanted into patients for therapeutic purposes without the removal of the sNAG nanofibers prior to cell transplantation.

SPECIFIC AIM-1

The goal of the first aim was to gain preliminary insights into the effects of sNAG nanofibers on UCB-EPC and hMVEC-C microtissue spheroid assembly and function *in vitro* under both 2D and 3D culture conditions. In particular, the biological response of endothelial cells to the instructive topography of sNAG nanofiber matrices was investigated by analyzing EC phenotype and morphology using bright field and confocal microscopy.

In general, the dynamic state, functions, and phenotype of ECs are regulated by highly complex temporal and spatial coordination of cell-cell and cell-substrate

interactions detected by cell receptors and integrated by cellular signaling pathways. Many of these events are mediated via cell adhesion proteins that form bonds with the cell's surface integrins, specifically a5b1 and aVb3, which induce firm adhesion at the cell-substrate interface. In previous studies, sNAG nanofibers have been shown to up-regulate a5b1 and aVb3 expression in ECs, which activates a series of downstream signaling pathways, including a Rac-dependent pathway generally thought to result in migration, MAP kinase (proliferation), PI3K/Akt (survival) and IKK/NFkB (survival). Although the exact mechanism by which sNAG nanofibers effect ECs in vitro is unknown, many of these pathways are known to be mediated through integrin dependent outside-in signal transduction. Therefore, to further investigate the effects of sNAG nanofibers on UCB-EPCs function in vitro, we tested the hypothesis that sNAG nanofiber topographies would provide an optimal or instructive interface for inducing UCB-EPC differentiation and will enhance assembly into tube-like structures *in vitro.*

To test this hypothesis, 2D Matrigel tube formation assays were performed. Qualitative analysis of UCB-EPCs show cellular adherence and spreading over the surface of sNAG 10ug/ml and 100ug/ml treated Matrigel cultures. Quantitative analysis of sprout and branch points support these observations. Results show a significant increase in sprout formation in sNAG 10 ug/ml treated cultures compared to 50ng/ml VEGF, suggesting a robust angiogenic EC response to sNAG nanofiber topographic cues. Additionally, sNAG 100 ug/ml treated cultures demonstrated a strong trend in the formation of branching capillary-like networks, suggesting a high degree of EC network remodeling after only 7 hours. Results of this assay demonstrate that by varying the

culture concentrations of sNAG nanofibers, ECs will undergo a differential response to the formation of tube-like networks. This effect may be due to the temporo-specific preference of ECs to different surface topography's during this dynamic process. However, it is unclear whether the effect of sNAG nanofibers on EC morphology during tube-like network formation is the result of increased rigidity of the Matrigel gels, whether it is due to increased a5b1 and aVb3 presentation (adhesion), or whether it is due cellular dimensionality (i.e. 2D versus 3D culture). More studies are needed to elucidate the specific sNAG matrix parameters that mediate EC morphogenesis in this assay.

Three-dimensional cell culture systems have gained increasing interest in drug discovery and tissue engineering due to their evident advantages in providing more physiologically relevant information and more predictive data for *in vivo* tests. Although our 2D Matrigel assay mentioned above provided valuable information regarding the effects of sNAG on EC tube-like network formation and function, 2D cell culture tests are limited in that they sometimes provide misleading and non-predictive data for *in vivo* responses. We, thus, developed a 3D culture system to study the effects of sNAG nanofibers on EC assembly and function in homotypic spheroid microtissues. We hypothesized that the addition of sNAG nanofiber substrates to suspension cultures of anchorage-dependent UCB-EPCs, it would promote spheroid formation by enhancing cellular adhesion in addition to cell-cell interactions.

hPECAM-1 is a membrane glycoprotein found at endothelial intercellular junctions and has been shown to mediate cell-cell interactions. In this study, the

morphology of attached ECs is considered to be an indication of cell adhesion with spread morphology indicating greater adhesion than round morphology. hPECAM-1 expression by endothelial cells was characterized using immunofluorescence confocal microscopy in cross-section and whole-mount microtissue spheroids. Results suggest that ECs in sNAG 10ug/ml microtissue spheroids provided the optimal concentration of nanofibers to induce cell migration toward the outer periphery of the modules. In contrast, sNAG 100ug/ml treated spheroids impeded cell migratory events, possibly due to phenomenon of durotaxis. Once ECs migrated toward the outer surface of the microtissue spheroids, ECs established a polarized elongated continuous monolayer after 1 day in cell culture. This is evidenced by increased hPECAM-1 expression intensity, which is indicative of a differentiated EC phenotype. Importantly, the differentiation characteristics of this surface monolayer go beyond the degree of differentiation that was obtained in our 2D Matrigel culture.

In conclusion, the addition of nanofiber fragments to suspension cultures of anchorage dependent ECs promoted spheroid formation. Spheroid formation in culture without nanofibers may be mediated by interactions among cadherins on adjacent cells. In contrast, in nanofiber supplemented culture, spheroid formation is also mediated by cell binding to the nanofibers. In this case, it is possible that vitronectin (aVb3 receptor) and fibronectin (a5b1 receptor) from the serum added to the culture medium are absorbed on the nanofibers, and then the cells adhere to these nanofibers, thereby forming spheroids. The higher efficiency of spheroid formation in nanofiber-supplemented culture may be due to the enhancement of EC assembly by nanofibers.

The conclusions in this aim are supported by (a) the observed polarized expression of endothelial cell surface molecules (basal and lateral expression of h-PECAM1 at the microtissue spheroid periphery), and (b) the ultrastructural characteristics of the surface monolayer with well-developed cell-cell contacts, and (c) assembly and alignment of ECs into primitive vessel-like structures in sNAG treated 3D cultures. Future studies will need to focus on analyzing the effects of sNAG nanofibers in both 2D and 3D environments and determining spheroid permeability in order to gain a better understanding of sNAG nanofiber influence on EC cell-cell junction formation.

Specific Aim-2

In the second aim, we focused not only on the initial assembly of vascular spheroids, but on the expansion and stabilization of these modules to include robust vascular networks. To do this, we tested whether sNAG nanofibers induced physiologic alignment and organization of vascular cell types, whether sNAG nanofibers facilitated recruitment of mural cells to nascent vascular structures, and whether sNAG nanofibers augmented vessel stabilization via synthesis and deposition of basement membrane proteins. We hypothesized that sNAG nanofibers would enhance vascular spheroid formation via heterotypic interactions between vascular cell types leading to the assembly of a mature and stabilized vascular network.

Previous experiments performed in aim-1 demonstrated that UCB-EPCs treated with sNAG nanofibers enhanced cell-cell junction formation and clustering of ECs into what appeared to be primitive vascular networks. The present study confirmed previous

observations that EC-only cultures demonstrate limited vascular network formation. The combination of UCB-EPCs and ADSC-VSMCs with sNAG nanofibers led to the development of remarkably complex vascular networks with a wide range of vessel geometries. These observations supported our theory that ADSC-VSMCs are able to behave as pericyte-like cells in our microtissue spheroid model by engaging in molecular cross-talk with ECs to induce vascular network formation. Furthermore, we found that aSMA antigen expression by ADSC-VSMCs was upregulated by day 3 in sNAG treated cultures, but the factors responsible for this effect were undefined. Heterotypic microtissue spheroids show that ADSC-VSMCs that were adjacent to UCB-EPCs specifically displayed induction of aSMA expression and its organization into contractile fibers. Thus, initial experiments suggest that sNAG nanofiber topography has an effect on EC assembly into vascular tubes and ADSC-VSMC differentiation over time.

When ECM protein expression and deposition were examined, we observed striking differences between control and sNAG treated microtissue spheroids. Among the large number of possible target for analysis of ECM proteins, we chose well-documented and essential components of the vascular wall ECM: collagen types I and IV. We note that our findings center on the deposition and structural organization of ECM proteins as they relate to vascular tissue engineering. As such, our primary means of analysis was immunofluorescence as it is the most reliable method to document, quantify, and distinguish proteins. This approach has been widely utilized in the analysis of ECM deposition.

Results show that collagen type-1 in sNAG nanofiber treated cultures was up-regulated in day-1 cultures compared to controls. However, by day-3 sNAG treated microtissue spheroids, a significant reduction of collagen type-1 was observed. One possibility for this finding is that collagen I is known to be produced by cells undergoing angiogenesis, which could have been halted by day 3 cultures reminiscent of a quiescent EC phenotype. Another possibility is that vascular collagen I may primarily be produced by synthetic SMCs, which could have retained a contractile phenotype by day 3. This possibility is further supported by the previous experiment where aSMA expression in sNAG treated cultures was up-regulated in day 3 cultures. Overall, these studies suggest that sNAG nanofibers have an effect on spheroid maturation events leading to variable production of collagen type 1.

Furthermore, we show that sNAG nanofibers mediate vascular morphogenesis leading to EC tube and vascular guidance tunnel formation. Vascular guidance tunnels serve as a critical matrix conduit for the recruitment and migration of pericytes along the abluminal surface of EC-lined tubes. In turn, these dynamic events resulted in continuous deposition of EC basement membrane proteins (i.e. collagen type-4). This process is a necessary step in the progression of tube assembly toward maturation and stabilization. Because pericyte coverage of EC tubes is more abundant in sNAG 100ug/ml cultures, this may represent the optimal concentration for assembly of prevascularized microtissue spheroids. Thus, it is likely that sNAG mediated EC-pericyte interactions, which catalyze vascular basement membrane matrix assembly, establish a matrix microenvironment that anchors and spatially organizes these cells into functional

structures. sNAG modified microtissue spheroids therefore lead to unique EC and pericyte signaling events that are necessary for vascular tube maturation and stabilization.

In conclusion, the addition of sNAG nanofiber fragments to 3D micro-mold cultures of EC-ADSC-VSMCs promoted spheroid formation. Our data suggest that EC-pericyte interactions are necessary for vascular tube assembly, maturation and stabilization in sNAG treated microtissue spheroids through basement membrane remodeling events, and through key changes in EC and pericyte integrin expression that facilitate recognition of these nanofibers. These changes most likely act in conjunction with growth factor-signaling pathways, mediated by sNAG nanofibers, to provide unique signals that are necessary for the transition from vascular tube morphogenesis to stabilization.

References:

1. Mozaffarian, D., et al., *Heart Disease and Stroke Statistics-2016 Update: A Report From the American Heart Association.* Circulation, 2016. **133**(4): p. e38-60.
2. Minino, A.M., et al., *Deaths: final data for 2008.* National vital statistics reports : from the Centers for Disease Control and Prevention, National Center for Health Statistics, National Vital Statistics System, 2011. **59**(10): p. 1-126.
3. Heidenreich, P.A., et al., *Forecasting the future of cardiovascular disease in the United States: a policy statement from the American Heart Association.* Circulation, 2011. **123**(8): p. 933-44.
4. Matas, A.J., et al., *OPTN/SRTR 2011 Annual Data Report: kidney.* American journal of transplantation : official journal of the American Society of Transplantation and the American Society of Transplant Surgeons, 2013. **13 Suppl 1**: p. 11-46.
5. Sun, Q., Z. Zhang, and Z. Sun, *The potential and challenges of using stem cells for cardiovascular repair and regeneration.* Genes & Diseases, 2014. **1**(1): p. 113-119.
6. Kovacic, J.C., R.P. Harvey, and S. Dimmeler, *Cardiovascular Regenerative Medicine: Digging In for the Long Haul.* Cell Stem Cell, 2007. **1**(6): p. 628-633.
7. Chen, C.W., et al., *Human pericytes for ischemic heart repair.* Stem cells, 2013. **31**(2): p. 305-16.
8. Dai, W., et al., *Allogeneic mesenchymal stem cell transplantation in postinfarcted rat myocardium: short- and long-term effects.* Circulation, 2005. **112**(2): p. 214-23.
9. Davani, S., et al., *Mesenchymal progenitor cells differentiate into an endothelial phenotype, enhance vascular density, and improve heart function in a rat cellular cardiomyoplasty model.* Circulation, 2003. **108 Suppl 1**: p. II253-8.
10. Suuronen, E.J., et al., *Comparative effects of mesenchymal progenitor cells, endothelial progenitor cells, or their combination on myocardial infarct regeneration and cardiac function.* The Journal of thoracic and cardiovascular surgery, 2007. **134**(5): p. 1249-58.
11. Agbulut, O., et al., *Comparison of human skeletal myoblasts and bone marrow-derived CD133+ progenitors for the repair of infarcted myocardium.* Journal of the American College of Cardiology, 2004. **44**(2): p. 458-463.
12. Dimmeler, S. and A.M. Zeiher, *Wanted! The best cell for cardiac regeneration.* Journal of the American College of Cardiology, 2004. **44**(2): p. 464-6.
13. Bianco, P., et al., *Bone Marrow Stromal Stem Cells: Nature, Biology, and Potential Applications.* STEM CELLS, 2001. **19**(3): p. 180-192.
14. Leeper, N.J., A.L. Hunter, and J.P. Cooke, *Stem cell therapy for vascular regeneration: Adult, Embryonic, and Induced Pluripotent Stem Cells.* Circulation, 2010. **122**(5): p. 517-526.
15. Lindahl, P., et al., *Pericyte loss and microaneurysm formation in PDGF-B-deficient mice.* Science, 1997. **277**(5323): p. 242-5.

16. Hellstrom, M., et al., *Lack of pericytes leads to endothelial hyperplasia and abnormal vascular morphogenesis.* The Journal of cell biology, 2001. **153**(3): p. 543-53.
17. Cheung, C. and S. Sinha, *Human embryonic stem cell-derived vascular smooth muscle cells in therapeutic neovascularisation.* Journal of molecular and cellular cardiology, 2011. **51**(5): p. 651-64.
18. Chang, W., B.-W. Song, and K.-C. Hwang, *Mesenchymal Stem Cell Survival in Infarcted Myocardium: Adhesion and Anti-death Signals*, in *Stem Cells and Cancer Stem Cells, Volume 10: Therapeutic Applications in Disease and Injury*, M.A. Hayat, Editor 2013, Springer Netherlands: Dordrecht. p. 35-43.
19. Michel, J.B., *Anoikis in the cardiovascular system: known and unknown extracellular mediators.* Arteriosclerosis, thrombosis, and vascular biology, 2003. **23**(12): p. 2146-54.
20. Taddei, M.L., et al., *Anoikis: an emerging hallmark in health and diseases.* The Journal of Pathology, 2012. **226**(2): p. 380-393.
21. Lee, S., et al., *Cell adhesion and long-term survival of transplanted mesenchymal stem cells: a prerequisite for cell therapy.* Oxidative medicine and cellular longevity, 2015. **2015**: p. 632902.
22. de Vos, P., et al., *Alginate-based microcapsules for immunoisolation of pancreatic islets.* Biomaterials, 2006. **27**(32): p. 5603-5617.
23. Guilak, F., et al., *Control of stem cell fate by physical interactions with the extracellular matrix.* Cell stem cell, 2009. **5**(1): p. 17-26.
24. Xiong, Q., et al., *A fibrin patch-based enhanced delivery of human embryonic stem cell-derived vascular cell transplantation in a porcine model of postinfarction left ventricular remodeling.* Stem cells, 2011. **29**(2): p. 367-75.
25. Rouwkema, J., N.C. Rivron, and C.A. van Blitterswijk, *Vascularization in tissue engineering.* Trends in Biotechnology. **26**(8): p. 434-441.
26. Dean, D.M., et al., *Rods, tori, and honeycombs: the directed self-assembly of microtissues with prescribed microscale geometries.* FASEB journal : official publication of the Federation of American Societies for Experimental Biology, 2007. **21**(14): p. 4005-12.
27. Yeh, J., et al., *Micromolding of shape-controlled, harvestable cell-laden hydrogels.* Biomaterials, 2006. **27**(31): p. 5391-8.
28. L'Heureux, N., T.N. McAllister, and L.M. de la Fuente, *Tissue-Engineered Blood Vessel for Adult Arterial Revascularization.* New England Journal of Medicine, 2007. **357**(14): p. 1451-1453.
29. Mironov, V., et al., *Organ printing: computer-aided jet-based 3D tissue engineering.* Trends in Biotechnology. **21**(4): p. 157-161.
30. McGuigan, A.P., B. Leung, and M.V. Sefton, *Fabrication of cells containing gel modules to assemble modular tissue-engineered constructs.* Nat. Protocols, 2007. **1**(6): p. 2963-2969.
31. L'Heureux, N., et al., *A completely biological tissue-engineered human blood vessel.* FASEB journal : official publication of the Federation of American Societies for Experimental Biology, 1998. **12**(1): p. 47-56.

32. Du, Y., et al., *Directed assembly of cell-laden microgels for fabrication of 3D tissue constructs.* Proceedings of the National Academy of Sciences, 2008. **105**(28): p. 9522-9527.
33. Nichol, J.W. and A. Khademhosseini, *Modular Tissue Engineering: Engineering Biological Tissues from the Bottom Up.* Soft matter, 2009. **5**(7): p. 1312-1319.
34. Lim, F. and A.M. Sun, *Microencapsulated islets as bioartificial endocrine pancreas.* Science, 1980. **210**(4472): p. 908-910.
35. Mano, J.F., et al., *Natural origin biodegradable systems in tissue engineering and regenerative medicine: present status and some moving trends.* Journal of the Royal Society Interface, 2007. **4**(17): p. 999-1030.
36. Grevenstein, J., et al., *Cartilage changes in rats induced by papain and the influence of treatment with N-acetylglucosamine.* Acta orthopaedica Belgica, 1991. **57**(2): p. 157-61.
37. Hirsch, J.A., et al., *Non-invasive hemostatic closure devices: “Patches and pads&#x201d.* Techniques in Vascular & Interventional Radiology. **6**(2): p. 92-95.
38. Palmer, B.L., et al., *Effectiveness and safety of manual hemostasis facilitated by the SyvekPatch with one hour of bedrest after coronary angiography using six-French catheters.* The American Journal of Cardiology, 2004. **93**(1): p. 96-97.
39. Pietramaggiori, G., et al., *Effects of poly-N-acetyl glucosamine (pGlcNAc) patch on wound healing in db/db mouse.* The Journal of trauma, 2008. **64**(3): p. 803-8.
40. Vournakis, J.N., et al., *Poly-N-acetyl glucosamine nanofibers regulate endothelial cell movement and angiogenesis: dependency on integrin activation of Ets1.* Journal of vascular research, 2008. **45**(3): p. 222-32.
41. Scherer, S.S., et al., *Poly-N-acetyl glucosamine nanofibers: a new bioactive material to enhance diabetic wound healing by cell migration and angiogenesis.* Annals of surgery, 2009. **250**(2): p. 322-30.
42. Beeson, C.C., et al., *Integrin-dependent Akt1 activation regulates PGC-1 expression and fatty acid oxidation.* Journal of vascular research, 2012. **49**(2): p. 89-100.
43. Lindner, H.B., et al., *Anti-Bacterial Effects of Poly-N-Acetyl-Glucosamine Nanofibers in Cutaneous Wound Healing: Requirement for Akt1.* PLoS ONE, 2011. **6**(4): p. e18996.
44. Fischer, T.H., et al., *Comparison of structural and hemostatic properties of the poly-N-acetyl glucosamine Syvek Patch with products containing chitosan.* Microscopy research and technique, 2004. **63**(3): p. 168-74.
45. Smith, C.J., et al., *Differential effect of materials for surface hemostasis on red blood cell morphology.* Microscopy research and technique, 2008. **71**(10): p. 721-9.
46. Ross, J.J., et al., *Cytokine-induced differentiation of multipotent adult progenitor cells into functional smooth muscle cells.* The Journal of clinical investigation, 2006. **116**(12): p. 3139-49.